

Anderson Acceleration in Nonsmooth Problems: Local Convergence via Active Manifold Identification

Kexin Li* Luwei Bai* Xiao Wang[†] Hao Wang[‡]

October 16, 2024

Abstract

Anderson acceleration is an effective technique for enhancing the efficiency of fixed-point iterations; however, analyzing its convergence in nonsmooth settings presents significant challenges. In this paper, we investigate a class of nonsmooth optimization algorithms characterized by the active manifold identification property. This class includes a diverse array of methods such as the proximal point method, proximal gradient method, proximal linear method, proximal coordinate descent method, Douglas-Rachford splitting (or the alternating direction method of multipliers), and the iteratively reweighted ℓ_1 method, among others. Under the assumption that the optimization problem possesses an active manifold at a stationary point, we establish a local R-linear convergence rate for the Anderson-accelerated algorithm. Our extensive numerical experiments further highlight the robust performance of the proposed Anderson-accelerated methods.

1 Introduction

In this paper, we focus on the following optimization problem:

$$\min_{\mathbf{x} \in \mathbb{R}^n} F(\mathbf{x}), \quad (1)$$

where, unless stated otherwise, $F : \mathbb{R}^n \rightarrow \mathbb{R} \cup \{\infty\}$ is assumed to be a closed and level-bounded function, potentially nonsmooth and composed of both smooth and nonsmooth terms. Such problems commonly arise in various fields, including statistics, signal processing, and machine learning. Depending on the specific characteristics of these problems, a diverse range of optimization algorithms has been developed. These include the proximal point algorithm, proximal gradient algorithm, proximal linear algorithm, and the Douglas-Rachford splitting algorithm, among others. A key feature of these algorithms is that their iterative schemes can often be reformulated as a fixed-point iteration for the following problem:

$$\text{Find } \mathbf{x} \in \mathbb{R}^n \text{ such that } \mathbf{x} = H(\mathbf{x}), \quad (2)$$

where $H : \mathbb{R}^n \rightarrow \mathbb{R}^n$ is a continuous mapping. For convex optimization problems, the mapping H is typically nonexpansive, and the solution set of (2) either coincides with or is closely related to the solution set of the original optimization problem.

*School of Information Science and Technology, ShanghaiTech University, Shanghai, People's Republic of China. Emails: likx0403@gmail.com, bailw@shanghaitech.edu.cn

[†]Department of AI Computing, Peng Cheng Laboratory, Shenzhen, People's Republic of China. Emails: wangx07@pcl.ac.cn

[‡]Corresponding author. School of Information Science and Technology, ShanghaiTech University, Shanghai, People's Republic of China. Emails: wanghao1@shanghaitech.edu.cn

Anderson acceleration is a widely recognized technique known for its effectiveness in enhancing the convergence of fixed-point problems, particularly in the later stages of iteration. By leveraging information from previous iterations, it combines weighted past iterations to generate a new one. Originally introduced to accelerate the iteration process of nonlinear integral equations, this method has since been extended to general fixed-point problems [36]. Anderson acceleration has been extensively studied and applied, yielding promising results in practical computations.

Despite its notable efficiency and widespread application, the theoretical convergence analysis of Anderson acceleration lags significantly behind its practical use. Counterexamples indicate that global convergence may fail under relatively mild conditions. Many studies have focused on its local convergence and rate. However, proving local convergence in the absence of continuous differentiability is particularly challenging, even though Anderson acceleration does not require derivatives. Local R-linear convergence has been established for the linear mapping [36], the continuously differentiable mapping [9], and the Lipschitz continuously differentiable mapping [36].

For nonsmooth problem, contemporary research frequently incorporates strategies such as restarting and safeguarding steps to ensure convergence. Safeguarded Anderson-accelerated variants have been proposed for several algorithms, including the proximal gradient algorithm [27], coordinate descent algorithm [3], and Douglas-Rachford splitting algorithm [17, 30]. However, these globalized algorithms always fail to provide complexity guarantees. There is still a lack of theoretical analysis to explain the superior local performance of Anderson acceleration in nonsmooth optimization algorithms. To our knowledge, existing studies guarantee local linear convergence rates for Anderson acceleration algorithms only for certain specific nonsmooth problems. For example, Bian et al. [5] study a fixed-point problem (with solution \mathbf{x}^*) decomposed into a smooth and a nonsmooth component with a small Lipschitz constant (where the constant approaches 0 as $\mathbf{x} \rightarrow \mathbf{x}^*$), demonstrating local linear convergence. Additionally, Bian and Chen [4] consider a class of nonsmooth composite fixed-point problems $\mathbf{x} = H(\mathbf{x}) := (F \circ P_\Omega \circ Q)(\mathbf{x})$, where F and Q are Lipschitz continuously differentiable and P_Ω is a box set projection. They smooth H and prove linear convergence for the Anderson-accelerated smoothing approximation. Mai and Johansson [27] propose an Anderson-accelerated proximal gradient (forward-backward splitting) algorithm with a local linear convergence rate guarantee. However, their method exclusively accelerates the forward step, the smooth part of the iteration—i.e., for a composite function $F := f + g$ where f is smooth and g is nonsmooth. The Anderson acceleration is applied only to the forward step $\mathbf{x}^{k+1/2} = \mathbf{x}^k - \nabla f(\mathbf{x}^k)/L$, while the backward step $\mathbf{x}^{k+1} = \text{prox}_{\beta g}(\mathbf{x}^{k+1/2})$, the nonsmooth part, remains unaccelerated.

Contributions. In this paper, we present a general theoretical framework for analyzing the local convergence rates of Anderson acceleration applied to various nonsmooth optimization algorithms that possess the active manifold identification property. These algorithms include the proximal point algorithm (PPA), proximal gradient algorithm (PGA), proximal linear algorithm (PLA), proximal coordinate descent algorithm (PCD), Douglas-Rachford splitting algorithm (DRS), alternating direction method of multipliers (ADMM), and the iteratively reweighted ℓ_1 algorithm (IRL1), among others, all of which tackle a wide range of nonsmooth optimization problems. We establish the local smoothness of iteration mappings for these algorithms, utilizing the corresponding theoretical framework. Additionally, we demonstrate local R-linear convergence rates for Anderson-accelerated versions of these algorithms. Figure 1 illustrates the structure of our theoretical analysis, while Table 1 summarizes the current progress and convergence results for the listed algorithms. Finally, we validate our theoreti-

cal findings and showcase the strong performance of Anderson-accelerated algorithms in our experiments.

| | PPA/PLA | PGA | PCD | DRS /ADMM | IRL1 |
|------------------------|---------|------------|------|-----------|------|
| Global convergence | - | [27] | [3] | [17, 30] | - |
| Local convergence rate | Ours | Ours, [27] | Ours | Ours | Ours |

Table 1: Comparison with existing Anderson accelerations in nonsmooth settings

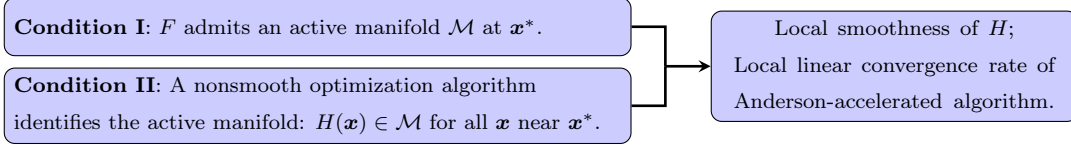


Figure 1: Flow of theoretical analysis to Anderson-accelerated nonsmooth optimization algorithms for (1) with \mathbf{x}^* being a Clarke critical point.

2 Notation and preliminaries

We denote $\mathbb{N} := \{0, 1, 2, \dots\}$ and \mathbb{R}_+^n as the nonnegative orthant in \mathbb{R}^n , with \mathbb{R}_{++}^n representing its interior. The norm $\|\mathbf{x}\|_p = (\sum_{i=1}^n |x_i|^p)^{1/p}$ is defined for $p \in (0, +\infty)$, and unless otherwise specified, $\|\cdot\|$ refers to the ℓ_2 norm. The function $\text{sign}(\mathbf{x})$ returns the element-wise sign of \mathbf{x} , i.e., $\text{sign}(\mathbf{x}) = [\text{sign}(x_1), \dots, \text{sign}(x_n)]^T$, and $\text{diag}(\mathbf{x}) \in \mathbb{R}^{n \times n}$ is the diagonal matrix with the elements of \mathbf{x} on its diagonal. Let $\mathcal{B}_{\mathbf{x}}(\rho)$ and $\hat{\mathcal{B}}_{\mathbf{x}}(\rho)$ denote the closed and open neighborhoods of \mathbf{x} with radius $\rho > 0$. We use $\nabla f(\mathbf{x})$ to denote the gradient of f at \mathbf{x} , and $\nabla_i f(\mathbf{x})$ to denote the partial derivative with respect to x_i , i.e., $\frac{\partial f(\mathbf{x})}{\partial x_i}$. A function $f : \mathbb{R}^n \rightarrow \mathbb{R} \cup \{\infty\}$ is called σ -weakly convex if the quadratically perturbed function $\mathbf{x} \mapsto f(\mathbf{x}) + \frac{\sigma}{2}\|\mathbf{x}\|^2$ is convex. Its *epigraph* is defined as $\text{epi} f := \{(\mathbf{x}, r) \in \mathbb{R}^n \times \mathbb{R} \mid r \geq f(\mathbf{x})\}$. For a set $\mathcal{M} \subseteq \mathbb{R}^n$, the indicator function $\chi_{\mathcal{M}}$ takes the value 0 in \mathcal{M} and $+\infty$ otherwise. A mapping $H : \mathbb{R}^n \rightarrow \mathbb{R}^n$ is called a *contraction* if there exists a constant $\gamma \in (0, 1)$ such that $\|H(\mathbf{x}) - H(\mathbf{y})\| \leq \gamma\|\mathbf{x} - \mathbf{y}\|$ for all $\mathbf{x}, \mathbf{y} \in \mathbb{R}^n$. The Jacobian matrix of a mapping $G : \mathbb{R}^n \rightarrow \mathbb{R}^m$ is denoted by ∇G , and \mathbb{I}_d represents the identity mapping from \mathbb{R}^d to \mathbb{R}^d . For a set S , the *relative interior* $\text{rint}(S)$ is defined as:

$$\text{rint}(S) := \{\mathbf{x} \in S : \text{there exists } \epsilon > 0 \text{ such that } \hat{\mathcal{B}}_{\mathbf{x}}(\epsilon) \cap \text{aff}(S) \subseteq S\},$$

where $\text{aff}(S)$ is the affine hull of S . Given a function $f : \mathbb{R}^n \rightarrow \mathbb{R} \cup \{\infty\}$ and a matrix $C \in \mathbb{R}^{m \times n}$, the *image function* $(Cf) : \mathbb{R}^m \rightarrow \mathbb{R} \cup \{\infty\}$ is defined as: $(Cf)(\mathbf{s}) := \inf_{\mathbf{x} \in \mathbb{R}^n} \{f(\mathbf{x}) \mid C\mathbf{x} = \mathbf{s}\}$.

2.1 Anderson acceleration

Consider the fixed-point problem (2), and let \mathbf{x}^* be its solution, i.e., a fixed point of H . The framework for Anderson-accelerated fixed-point iterations is described in Algorithm 1.

In Algorithm 1, we define $H^k = H(\mathbf{x}^k)$, $\mathbf{r}^k = H(\mathbf{x}^k) - \mathbf{x}^k$ as the residue, and $R^k = [\mathbf{r}^k, \dots, \mathbf{r}^{k-m_k}]$ for $k \geq 0$. Starting with an initial point \mathbf{x}^0 and an integer $m \geq 1$, the key step in Anderson acceleration (Step 5) involves calculating the weight vector $\boldsymbol{\alpha}^k \in \mathbb{R}^{m_k+1}$ that minimizes the weighted sum of the previous $m_k + 1$ residues. It is straightforward to see that

Algorithm 1 Anderson acceleration

- 1: Given $\mathbf{x}^0 \in \mathbb{R}^n$ and integer $m \geq 1$.
 - 2: Set $k = 0$, $H^0 = H(\mathbf{x}^0)$, and $\mathbf{r}^0 = H^0 - \mathbf{x}^0$.
 - 3: **while** not convergent **do**
 - 4: Set $m_k = \min(m, k)$ and $R^k = [\mathbf{r}^k, \dots, \mathbf{r}^{k-m_k}]$
 - 5: Compute $\boldsymbol{\alpha}^k = \arg \min_{\boldsymbol{\alpha}^T \mathbf{e} = 1} \|\mathbf{R}^k \boldsymbol{\alpha}\|^2$
 - 6: Compute $\mathbf{x}^{k+1} = \sum_{i=0}^{m_k} \alpha_i^k H^{k-m_k+i}$
 - 7: Compute $H^{k+1} = H(\mathbf{x}^{k+1})$ and $\mathbf{r}^{k+1} = H^{k+1} - \mathbf{x}^{k+1}$
 - 8: Set $k = k + 1$
 - 9: **end while**
 - 10: **return** \mathbf{x}^k
-

$\boldsymbol{\alpha}^k$ can be explicitly expressed as [27]: $\boldsymbol{\alpha}^k = \frac{[(R^k)^T R^k]^{-1} \mathbf{1}}{\mathbf{1}^T [(R^k)^T R^k]^{-1} \mathbf{1}}$. The computational cost of Step 5 is $O(m_k^2 + nm_k)$. Given that m_k is typically a small integer in practice, such as 5 – 15, solving this subproblem incurs minimal computation. Therefore, Anderson acceleration does not significantly increase the computational burden. Furthermore, if $(R^k)^T R^k$ is singular, we can ensure the subproblem’s non-singularity by adding a Tikhonov regularization term $\tau \|\boldsymbol{\alpha}\|^2$ to the objective function [27], where $\tau > 0$ is a small constant.

In this paper, we make the following assumption regarding the fixed-point mapping H and the coefficients generated by Anderson acceleration.

Assumption A1. *Let \mathbf{x}^* be the solution of the fixed-point problem $\mathbf{x} = H(\mathbf{x})$ and let $\{\boldsymbol{\alpha}^k\}$ denote the sequence generated by Anderson acceleration.*

- (i) *There exist constants $\rho, \gamma > 0$ such that $\|H(\mathbf{x}) - H(\mathbf{y})\| \leq \gamma \|\mathbf{x} - \mathbf{y}\|$ for all $\mathbf{x}, \mathbf{y} \in \mathcal{B}_{\mathbf{x}^*}(\rho)$*
- (ii) *There exists an upper bound M_α such that $\sum_{i=0}^{m_k} |\alpha_i^k| \leq M_\alpha$ for all $k \in \mathbb{N}$.*

These assumptions are commonly used in the literature on Anderson acceleration [4, 5, 36]. Assumption A1(ii) ensures the boundedness of $\sum_{i=0}^{m_k} |\alpha_i^k|$. In our experiments, we also observed this phenomenon. Although proving the boundedness remains elusive, several practical approaches have been proposed to ensure it [32, 36].

The first convergence result for Anderson acceleration is presented in [36, Theorem 2.3]. Under the assumption of Lipschitz continuous differentiability of H , Anderson acceleration guarantees R-linear convergence when initialized near the fixed point \mathbf{x}^* .

Theorem 1. *Under Assumption A1, suppose that H is Lipschitz continuously differentiable in a neighborhood $\mathcal{B}_{\mathbf{x}^*}(\hat{\rho})$ of \mathbf{x}^* for some $0 < \hat{\rho} \leq \rho$ and $\mathbf{x}^0 \in \mathcal{B}_{\mathbf{x}^*}(\hat{\rho})$. Then, when \mathbf{x}^0 is sufficiently close to \mathbf{x}^* , the iterates $\{\mathbf{x}^k\}$ generated by Anderson acceleration remain in $\mathcal{B}_{\mathbf{x}^*}(\hat{\rho})$ and converge to \mathbf{x}^* R-linearly with $\hat{\gamma} \in (\gamma, 1)$:*

$$\|H^k - \mathbf{x}^k\| \leq \hat{\gamma}^k \|H^0 - \mathbf{x}^0\| \quad \text{and} \quad \|\mathbf{x}^k - \mathbf{x}^*\| \leq \frac{1 + \gamma}{1 - \gamma} \hat{\gamma}^k \|\mathbf{x}^0 - \mathbf{x}^*\|. \quad (3)$$

2.2 Subdifferentials

The following concepts about subdifferentials are well-established in the literature, such as [11]. The regular (Fréchet) normal cone to a set $Q \subset \mathbb{R}^n$ at a point $\mathbf{x} \in \mathbb{R}^n$ is defined as follows:

$$N_Q(\mathbf{x}) := \left\{ \boldsymbol{\nu} \in \mathbb{R}^n : \limsup_{\mathbf{y} \rightarrow \mathbf{x}, \mathbf{y} \in Q} \frac{\langle \boldsymbol{\nu}, \mathbf{y} - \mathbf{x} \rangle}{\|\mathbf{y} - \mathbf{x}\|} \leq 0 \right\}.$$

The limiting normal cone to Q at $\mathbf{x} \in Q$, denoted by $\hat{N}_Q(\mathbf{x})$, is defined to consist of all vectors $\boldsymbol{\nu} \in \mathbb{R}^n$ for which there exist sequences $\mathbf{x}_i \in Q$ and $\boldsymbol{\nu}_i \in \hat{N}_Q(\mathbf{x}_i)$ satisfying $(\mathbf{x}_i, \boldsymbol{\nu}_i) \rightarrow (\mathbf{x}, \boldsymbol{\nu})$. The Clarke normal cone, denoted by $N_Q^c(\mathbf{x})$, is defined as the closed convex hull of $\hat{N}_Q(\mathbf{x})$. For all points $\mathbf{x} \in Q$, it holds that $N_Q(\mathbf{x}) \subset \hat{N}_Q(\mathbf{x}) \subset N_Q^c(\mathbf{x})$. Generalized gradients of a function can be defined through the normal cones to epigraphs. Specifically, consider a function $f : \mathbb{R}^n \rightarrow \mathbb{R} \cup \{\infty\}$ and a point \mathbf{x} such that $f(\mathbf{x})$ is finite. The subderivative $df(\mathbf{x})(\cdot)$ is defined by

$$df(\mathbf{x})(\bar{\boldsymbol{\nu}}) = \liminf_{\tau \downarrow 0} \inf_{\boldsymbol{\nu} \rightarrow \bar{\boldsymbol{\nu}}} \frac{f(\mathbf{x} + \tau \boldsymbol{\nu}) - f(\mathbf{x})}{\tau}, \quad \boldsymbol{\nu} \in \mathbb{R}^n.$$

The regular and Clarke subdifferentials of f at \mathbf{x} are respectively defined as

$$\begin{aligned} \partial f(\mathbf{x}) &:= \{\boldsymbol{\nu} \in \mathbb{R}^n : (\boldsymbol{\nu}, -1) \in N_{\text{epi}f}(\mathbf{x}, f(\mathbf{x}))\}, \\ \partial_c f(\mathbf{x}) &:= \{\boldsymbol{\nu} \in \mathbb{R}^n : (\boldsymbol{\nu}, -1) \in N_{\text{epi}f}^c(\mathbf{x}, f(\mathbf{x}))\}. \end{aligned}$$

A point $\bar{\mathbf{x}}$ satisfying $\mathbf{0} \in \partial f(\bar{\mathbf{x}})$ is called a *critical point* of f , and a point satisfying $\mathbf{0} \in \partial_c f(\bar{\mathbf{x}})$ is called a *Clarke critical point*. Notably, the latter requirement is much weaker than the former. The distinction disappears for weakly convex functions [11]. We say that f is (subdifferentially) regular at \mathbf{x} if $\text{epi}f$ is locally closed around \mathbf{x} and $N_Q(\mathbf{x}) = N_Q^c(\mathbf{x})$.

2.3 Weak convexity and Moreau envelope

For a σ -weakly convex function $f : \mathbb{R}^n \rightarrow \mathbb{R} \cup \{\infty\}$, it naturally has a lower bound:

$$f(\mathbf{y}) \geq f(\mathbf{x}) + \langle \boldsymbol{\nu}, \mathbf{y} - \mathbf{x} \rangle - \frac{\sigma}{2} \|\mathbf{y} - \mathbf{x}\|^2, \quad \forall \mathbf{x}, \mathbf{y} \in \mathbb{R}^n, \boldsymbol{\nu} \in \partial f(\mathbf{x}).$$

The Moreau envelope and proximal point mapping of f are defined as follows:

$$\begin{aligned} f_\beta(\mathbf{x}) &= \inf_{\mathbf{y} \in \mathbb{R}^n} \left\{ f(\mathbf{y}) + \frac{1}{2\beta} \|\mathbf{y} - \mathbf{x}\|^2 \right\}, \\ \text{prox}_{\beta f}(\mathbf{x}) &= \arg \min_{\mathbf{y} \in \mathbb{R}^n} \left\{ f(\mathbf{y}) + \frac{1}{2\beta} \|\mathbf{y} - \mathbf{x}\|^2 \right\}. \end{aligned}$$

In the following lemma, we summarize the basic properties that are used in this paper. More properties can be found in [10, Lemma 2.5].

Lemma 2.1. *Let $f : \mathbb{R}^d \rightarrow \mathbb{R} \cup \{\infty\}$ be a σ -weakly convex function, and fix a positive parameter $\beta < \sigma^{-1}$. The following statements hold:*

- (i) *The Moreau envelope f_β is \mathcal{C}^1 -smooth and $\frac{\sigma}{1-\beta\sigma}$ -weakly convex.*
- (ii) *The proximal mapping $\text{prox}_{\beta f}$ is $\frac{1}{1-\beta\sigma}$ -Lipschitz continuous.*
- (iii) *The critical points of f and f_β coincide, and they are exactly the fixed points of the proximal mapping $\text{prox}_{\beta f}$.*

2.4 Manifold optimization

Nonsmooth optimization problems often exhibit significant structure, with many studies demonstrating that the nonsmooth behavior of their objective functions is closely related to an active manifold in the local region [19, 22]. Specifically, the critical points of typical nonsmooth functions lie on a manifold, where the functions are smooth. This relationship allows us to explore

the local smoothness properties of nonsmooth optimization problems through the lens of manifold optimization. The concept of an active manifold is closely tied to the active set. From an algorithmic perspective, active manifolds are sets that typical algorithms can identify in finite time. The notion of active manifolds has been modeled in various ways, such as partly smooth manifolds [22], \mathcal{UV} -structures [28], $g \circ F$ decomposable functions [33], and minimal identifiable sets [12]. We first revisit the definition of a smooth manifold [10, Definition 2.2].

Definition 2.1 (Smooth manifold). *A subset $\mathcal{M} \subset \mathbb{R}^n$ is called a \mathcal{C}^p -smooth manifold (for $p \geq 1$) of dimension r around $\bar{\mathbf{x}} \in \mathcal{M}$ if there exists an open neighborhood $\hat{\mathcal{B}}_{\bar{\mathbf{x}}}(\epsilon)$ around $\bar{\mathbf{x}}$ with radius $\epsilon > 0$ and a mapping $G : \mathbb{R}^n \rightarrow \mathbb{R}^{n-r}$ such that:*

- (i) *G is \mathcal{C}^p -smooth.*
- (ii) *The Jacobian $\nabla G(\bar{\mathbf{x}})$ has full row rank.*
- (iii) *The following equality holds: $\mathcal{M} \cap \hat{\mathcal{B}}_{\bar{\mathbf{x}}}(\epsilon) = \{\mathbf{x} \in \hat{\mathcal{B}}_{\bar{\mathbf{x}}}(\epsilon) : G(\mathbf{x}) = \mathbf{0}\}$.*

We refer to $G(\mathbf{x}) = 0$ as the locally defined equation of \mathcal{M} .

We define the tangent and normal spaces to \mathcal{M} at \mathbf{x} as $T_{\mathcal{M}}(\mathbf{x}) := \text{Null}(\nabla G(\mathbf{x}))$ and $N_{\mathcal{M}}(\mathbf{x}) := (T_{\mathcal{M}}(\mathbf{x}))^\perp$. Next, we introduce the concept of a partly smooth function and an active manifold [22, Definition 2.7].

Definition 2.2 (Partly smooth function and active manifold). *Let $f : \mathbb{R}^n \rightarrow \mathbb{R} \cup \{\infty\}$ be a closed function, and $\mathcal{M} \subseteq \mathbb{R}^n$ be a set containing a point $\bar{\mathbf{x}}$. The function f is said to be partly smooth at $\bar{\mathbf{x}}$ relative to \mathcal{M} if:*

- (i) *(Smoothness) The set $\mathcal{M} \cap \hat{\mathcal{B}}_{\bar{\mathbf{x}}}(\epsilon)$ is a \mathcal{C}^p -smooth manifold, and the restriction of f to $\mathcal{M} \cap \hat{\mathcal{B}}_{\bar{\mathbf{x}}}(\epsilon)$ is \mathcal{C}^p -smooth.*
- (ii) *(Regularity) For all \mathbf{x} near $\bar{\mathbf{x}}$ in \mathcal{M} , f is regular and has a subgradient.*
- (iii) *(Normal sharpness) $dh(\mathbf{x})(-\boldsymbol{\nu}) > -dh(\mathbf{x})(\boldsymbol{\nu})$ for all nonzero $\boldsymbol{\nu}$ in $N_{\mathcal{M}}(\bar{\mathbf{x}})$.*
- (iv) *(Subgradient continuity) The subdifferential mapping $\partial_c f$ is continuous at $\bar{\mathbf{x}}$ relative to \mathcal{M} .*

The manifold \mathcal{M} is called a \mathcal{C}^p -active manifold, and f admits \mathcal{M} at $\bar{\mathbf{x}}$.

Partly smooth functions encompass a wide variety of functions, such as smooth functions, polyhedral functions, the indicator and distance functions of a smooth manifold \mathcal{M} , and the sum of a smooth function and a partly smooth function. A more detailed introduction is provided in [22]. Numerous examples, particularly in signal processing, machine learning, and statistics, are discussed in [37]. We summarize several examples in Table 2 [24]. Figure 2 illustrates the landscapes of several widely used nonsmooth functions. As shown, the ℓ_1 , $\ell_1 - \ell_2$, and ℓ_p functions admit a \mathcal{C}^∞ -active manifold at $(1, 0)$ with $\mathcal{M} = \{(x, y) : y = 0\}$. The ℓ_∞ function and TV regularization admit a \mathcal{C}^∞ -active manifold at $(1, 1)$ with $\mathcal{M} = \{(x, y) : x = y\}$. When restricted to \mathcal{M} at the considered points, these functions vary smoothly along \mathcal{M} locally, while grow sharply when moving normal to \mathcal{M} . We also introduce a class of nonconvex sparsity regularization functions that admit active manifolds in Table 4.

For a partly smooth function f and its active manifold \mathcal{M} , a key research question is whether an algorithm can identify the active manifold \mathcal{M} within a finite number of steps. To ensure this, the non-degeneracy condition $\mathbf{0} \in \text{rint } \partial_c f(\mathbf{x})$ is often imposed [24, 27]. As argued

| Function | Active manifold | Function | Active manifold |
|-----------------------------|--|------------------------------|---|
| $\ \cdot\ _1$ | $\{z \in \mathbb{R}^n : I_z \subseteq I_{\bar{x}}\}$ | $\ \cdot\ _\infty$ | $\{z \in \mathbb{R}^n : z_{J_{\bar{x}}} \in \mathbb{R}\text{sign}(\bar{x}_{J_{\bar{x}}})\}$ |
| $\ \cdot\ _1 - \ \cdot\ _2$ | $\{z \in \mathbb{R}^n : I_z \subseteq I_{\bar{x}}\}$ | $\ D_{\text{DIF}} \cdot\ _1$ | $\{z \in \mathbb{R}^n : I_{D_{\text{DIF}}z} \subseteq I_{D_{\text{DIF}}\bar{x}}\}$ |
| $\ \cdot\ _p^p$ | $\{z \in \mathbb{R}^n : I_z \subseteq I_{\bar{x}}\}$ | $\chi_{[l,u]}(\cdot)$ | $\{z \in \mathbb{R}^n : \forall \bar{x}_i = u_i \text{ or } l_i, z_i = \bar{x}_i\}$ |

Table 2: Common functions and their active manifolds \mathcal{M} at a given point \bar{x} . We define $I_{\bar{x}} = \{i : \bar{x}_i \neq 0\}$ and $J_{\bar{x}} = \{i : |\bar{x}_i| = \|\bar{x}\|_\infty\}$. We use $D_{\text{DIF}}\mathbf{x} = [0, x_2 - x_1, \dots, x_n - x_{n-1}]$ to represent the finite difference of \mathbf{x} [31]. The notation $\mathbb{R}\text{sign}(\mathbf{x}_{I_{\bar{x}}})$ refers to the span of $\text{sign}(\mathbf{x}_{I_{\bar{x}}})$, and $-\infty \leq l \leq u \leq +\infty$.

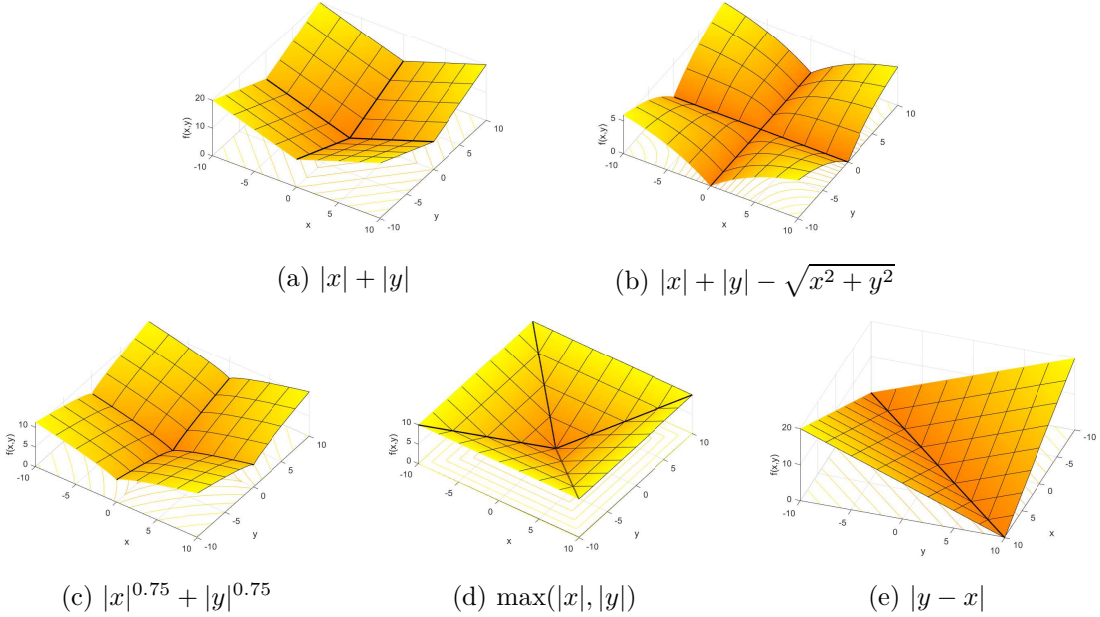


Figure 2: Landscapes of commonly used 2-dimensional nonsmooth functions $f(x, y)$.

in [19], this condition is nearly essential for guaranteeing the identification property. With the non-degeneracy condition, it has been shown that many algorithms can successfully identify the active manifold in a finite number of steps [1, 10, 19]. We now provide a formal definition:

Definition 2.3 (Active manifold identification). *Consider an algorithm solving problem (1), which generates a sequence $\mathbf{x}^k \rightarrow \bar{\mathbf{x}}$, and whose iterations follow the fixed-point scheme $\mathbf{x}^{k+1} = H(\mathbf{x}^k)$. Suppose that F admits an active manifold \mathcal{M} at $\bar{\mathbf{x}}$. Then, we say the algorithm identifies the active manifold \mathcal{M} if the inclusion $H(\mathbf{x}) \in \mathcal{M}$ holds for all \mathbf{x} near $\bar{\mathbf{x}}$.*

This property is crucial in the subsequent analysis, as it ensures the local smoothness of the iteration mappings defined for the algorithms under consideration. To proceed, we examine the family of optimization problems:

$$\zeta(\mathbf{x}) = \arg \min_{\mathbf{y} \in \{\mathbf{y} | G(\mathbf{x}, \mathbf{y}) = \mathbf{0}, J(\mathbf{x}, \mathbf{y}) \leq \mathbf{0}\}} v(\mathbf{x}, \mathbf{y}), \quad \text{and} \quad V(\mathbf{x}) = v(\mathbf{x}, \zeta(\mathbf{x})), \quad (4)$$

where $v : \mathbb{R}^n \times \mathbb{R}^d \rightarrow \mathbb{R} \cup \{\infty\}$, $G : \mathbb{R}^n \times \mathbb{R}^d \rightarrow \mathbb{R}^r$, and $J : \mathbb{R}^n \times \mathbb{R}^d \rightarrow \mathbb{R}^c$ are \mathcal{C}^p -smooth ($p \geq 2$). Following sensitivity analysis theory [16], particularly [16, Theorem 2.1, Corollary 4.1], we establish the local smoothness of $\zeta(\mathbf{x})$ and $V(\mathbf{x})$.

Lemma 2.2 (Sensitivity analysis). *Consider the problem in (4) and fix a point $\bar{\mathbf{x}} \in \mathbb{R}^n$. Suppose that $\zeta(\bar{\mathbf{x}})$ is a strong local minimizer and a unique global minimizer, and that $\zeta(\mathbf{x})$ varies continuously near $\bar{\mathbf{x}}$. If the Jacobian $\nabla_{\mathbf{y}} G(\bar{\mathbf{x}}, \zeta(\bar{\mathbf{x}}))$ has full row rank and the inequality constraint is inactive at $(\bar{\mathbf{x}}, \zeta(\bar{\mathbf{x}}))$, i.e., $J_i(\bar{\mathbf{x}}, \zeta(\bar{\mathbf{x}})) < 0$ for all $i = 1, \dots, c$, then $\zeta(\mathbf{x})$ is \mathcal{C}^{p-1} -smooth and $V(\mathbf{x})$ is \mathcal{C}^p -smooth for all \mathbf{x} near $\bar{\mathbf{x}}$.*

When considering Anderson acceleration for an algorithm solving problem (1), the key idea is to reformulate the iteration as a fixed-point iteration $\mathbf{x}^{k+1} = H(\mathbf{x}^k)$ and then apply Algorithm 1. By utilizing active manifold theory, we can offer a simplified convergence analysis for various algorithms. The active manifold identification property and Lemma 2.2 are pivotal. With these, we establish the local R-linear convergence rate for Anderson-accelerated algorithms. The central idea is to ensure the local smoothness of H , following the reasoning in [10]. Theorem 2 forms the foundation for the theoretical analysis in the subsequent sections.

Theorem 2. *Consider the problem (1), and let \mathbf{x}^* be a Clarke critical point of F . Suppose that F admits a \mathcal{C}^3 -active manifold \mathcal{M} at \mathbf{x}^* . Assume an algorithm generates a sequence $\mathbf{x}^k \rightarrow \mathbf{x}^*$, with iterations formulated as*

$$\mathbf{x}^{k+1} = H(\mathbf{x}^k), \quad \text{where} \quad H(\mathbf{x}) := \arg \min_{\mathbf{y} \in \mathbb{R}^n} s(\mathbf{x}, \mathbf{y}). \quad (5)$$

Here $s : \mathbb{R}^n \times \mathbb{R}^n \rightarrow \mathbb{R} \cup \{\infty\}$ inherits the \mathcal{C}^3 -smoothness of F on \mathcal{M} near \mathbf{x}^* . Assume that H is a unique strong global minimizer and the algorithm identifies \mathcal{M} , the following statements hold:

- (i) H is \mathcal{C}^2 -smooth, and both H and ∇H are Lipschitz continuous near \mathbf{x}^* .
- (ii) Under Assumption A1, if the initial point \mathbf{x}^0 is sufficiently close to \mathbf{x}^* , applying Anderson acceleration to (5) via Algorithm 1 yields iterates that converge to \mathbf{x}^* R-linearly with a rate $\hat{\gamma} \in (\gamma, 1)$, i.e., (3) holds.

Proof. (i) The active manifold identification property ensures that $H(\mathbf{x}) \in \mathcal{M}$ for all \mathbf{x} near \mathbf{x}^* . Thus, we can approach the analysis via sensitivity analysis. Let $\hat{s}(\mathbf{x}, \cdot)$ be a \mathcal{C}^3 -smooth

function that coincides with $s(\mathbf{x}, \cdot)$ on \mathcal{M} near \mathbf{x}^* . For any \mathbf{x} close to \mathbf{x}^* , we have

$$H(\mathbf{x}) = \arg \min_{\mathbf{y} \in \mathcal{M} \cap \mathcal{B}_{\mathbf{x}^*}(\hat{\rho})} \hat{s}(\mathbf{x}, \mathbf{y}), \quad (6)$$

where $0 < \hat{\rho} \leq \rho$. Then we are ready to apply Lemma 2.2 to the problem (6) with

$$\zeta(\mathbf{x}) := H(\mathbf{x}) \text{ and } v(\mathbf{x}, \mathbf{y}) := \hat{s}(\mathbf{x}, \mathbf{y}).$$

Additionally, by Definition 2.1 (iii), there exists a mapping $G^{\mathcal{M}} : \mathbb{R}^n \rightarrow \mathbb{R}^{n-r}$ such that $\mathcal{M} \cap \mathcal{B}_{\mathbf{x}^*}(\hat{\rho}) = \{\mathbf{x} \in \mathcal{B}_{\mathbf{x}^*}(\hat{\rho}) : G^{\mathcal{M}}(\mathbf{x}) = \mathbf{0}\}$. Hence,

$$\mathcal{M} \cap \mathcal{B}_{\mathbf{x}^*}(\hat{\rho}) = \{\mathbf{x} \in \mathbb{R}^n : G(\mathbf{x}, \mathbf{y}) = \mathbf{0}, J(\mathbf{x}, \mathbf{y}) \leq \mathbf{0}\},$$

where $G(\mathbf{x}, \mathbf{y}) := G^{\mathcal{M}}(\mathbf{y})$ and $J(\mathbf{x}, \mathbf{y}) := \|\mathbf{y} - \mathbf{x}^*\|^2 - \hat{\rho}^2$. Then we conclude that H is \mathcal{C}^2 -smooth near \mathbf{x}^* , which also implies that H and ∇H are Lipschitz continuous.

(ii) Building on the result from (i) and Assumption A1, there exists a neighborhood $\mathcal{B}_{\mathbf{x}^*}(\rho)$ of \mathbf{x}^* for some sufficiently small $\rho > 0$ such that $\|\nabla H(\mathbf{x})\| \leq \gamma$ for all $\mathbf{x} \in \mathcal{B}_{\mathbf{x}^*}(\rho)$. By Theorem 1, we establish the R-linear convergence of the Anderson-accelerated sequence, thus completing the proof. \square

3 Anderson-accelerated proximal algorithms

Our task in this section is to establish the theoretical properties of Anderson acceleration applied to three proximal algorithms for solving the non-smooth optimization problem:

$$\min_{\mathbf{x} \in \mathbb{R}^n} F(\mathbf{x}) := (f \circ h)(\mathbf{x}) + g(\mathbf{x}), \quad (7)$$

where $h : \mathbb{R}^n \rightarrow \mathbb{R}^d$ is \mathcal{C}^2 -smooth, $f : \mathbb{R}^d \rightarrow \mathbb{R}$ is convex, and $g : \mathbb{R}^n \rightarrow \mathbb{R} \cup \{\infty\}$ is closed and σ -weakly convex. Similar to [23], we assume that there exists $\eta > 0$ such that:

$$|f(h(\mathbf{y})) - f(h(\mathbf{x}) + \nabla h(\mathbf{x})(\mathbf{y} - \mathbf{x}))| \leq \frac{\eta}{2} \|\mathbf{y} - \mathbf{x}\|^2, \quad \forall \mathbf{x}, \mathbf{y} \in \mathbb{R}^n. \quad (8)$$

Problem (7) and its variants encompass a wide array of non-smooth optimization issues. In Table 3, we present three types of non-smooth optimization problems along with commonly used algorithms, including the proximal point algorithm [29], proximal gradient (Forward-Backward splitting) algorithm [2, 24], and proximal linear algorithm [23]. Each of these algorithms involves subproblems that can be represented as fixed-point iterations in the form (5).

| Alg. | $F(\mathbf{x})$ | $s(\mathbf{x}, \mathbf{y})$ |
|------|---|---|
| PPA | $g(\mathbf{x})$ | $g(\mathbf{y}) + \frac{1}{2\beta} \ \mathbf{y} - \mathbf{x}\ ^2$ |
| PGA | $h(\mathbf{x}) + g(\mathbf{x})$ | $h(\mathbf{x}) + \nabla h(\mathbf{x})(\mathbf{y} - \mathbf{x}) + g(\mathbf{y}) + \frac{1}{2\beta} \ \mathbf{y} - \mathbf{x}\ ^2$ |
| PLA | $(f \circ h)(\mathbf{x}) + g(\mathbf{x})$ | $f(h(\mathbf{x}) + \nabla h(\mathbf{x})(\mathbf{y} - \mathbf{x})) + g(\mathbf{y}) + \frac{1}{2\beta} \ \mathbf{y} - \mathbf{x}\ ^2$ |

Table 3: Three proximal-type algorithms for solving (7). PPA: Proximal point algorithm; PGA: Proximal gradient algorithm; PLA: Proximal linear algorithm

As illustrated in Table 3, the proximal linear algorithm generalizes both the proximal point algorithm (with $h \equiv 0$, $f \equiv 0$) and the proximal gradient algorithm (with $d = 1$, $f = \mathbb{I}_d$). Moreover, in the context of the proximal gradient algorithm, condition (8) can be inferred from the Lipschitz continuity of ∇h . We will focus on the proximal linear algorithm and provide a

convergence analysis for the Anderson-accelerated proximal linear algorithm. The results in Theorem 3 can also be applied to Anderson-accelerated proximal point and proximal gradient algorithms,

We are now ready to demonstrate the locally R-linear convergence rate of the Anderson-accelerated proximal linear algorithm. Theorem 2 plays a critical role in the subsequent analysis, enabling us to show the smoothness of the iteration mapping of the proximal linear algorithm around \mathbf{x}^* and establish the local R-linear convergence rate for the Anderson-accelerated proximal linear algorithm. Before presenting the main result of this section, we introduce the concept of the composite active manifold for the composite function F in problem (7), based on the active manifolds of f and g and the transversality condition—a fundamental notion in differential geometry that guarantees the intersection of two manifolds remains a manifold [21, Theorem 6.30] [10, Definition 5.1].

Definition 3.1 (Composite active manifold). *Consider the composite optimization problem (7). Let \mathbf{x}^* be a critical point of F . For any $\mathbf{w}^* \in \partial f(h(\mathbf{x}^*))$ and $\mathbf{v}^* \in \partial g(\mathbf{x}^*)$ satisfying $\mathbf{0} \in \nabla h(\mathbf{x}^*)^* \mathbf{w}^* + \mathbf{v}^*$, suppose the following conditions hold:*

- (i) *There exist \mathcal{C}^p -smooth manifolds $\mathcal{G} \subset \mathbb{R}^n$ and $\mathcal{F} \subset \mathbb{R}^d$ containing \mathbf{x}^* and $h(\mathbf{x}^*)$, respectively, satisfying the transversality condition:*

$$\nabla h(\mathbf{x}^*)[T_{\mathcal{G}}(\mathbf{x}^*)] + T_{\mathcal{F}}(h(\mathbf{x}^*)) = \mathbb{R}^d. \quad (9)$$

- (ii) *Non-degeneracy conditions $\mathbf{v}^* \in \text{rint}(\partial g(\mathbf{x}^*))$ and $\mathbf{w}^* \in \text{rint}(\partial f(h(\mathbf{x}^*)))$ hold.*

- (iii) *\mathcal{G} is an active manifold of g at \mathbf{x}^* , and \mathcal{F} is an active manifold of f at $h(\mathbf{x}^*)$.*

We say that F admits a \mathcal{C}^p -composite active manifold $\mathcal{M} := \mathcal{G} \cap h^{-1}(\mathcal{F})$ at \mathbf{x}^* .

According to Definition 3.1, to ensure that F admits an active manifold at \mathbf{x}^* , the nonsmooth functions g and f must admit active manifolds \mathcal{G} and \mathcal{F} at \mathbf{x}^* and $h(\mathbf{x}^*)$, respectively. The non-degeneracy conditions for f and g , along with the classical transversality condition (9) ensure $\mathbf{0} \in \text{rint}(\partial F(\mathbf{x}^*))$ [10].

Theorem 3. *Consider the composite optimization problem (7). Let \mathbf{x}^* be a critical point of F and let*

$$H(\mathbf{x}) = \arg \min_{\mathbf{y} \in \mathbb{R}^n} f(h(\mathbf{x}) + \nabla h(\mathbf{x})(\mathbf{y} - \mathbf{x})) + g(\mathbf{y}) + \frac{1}{2\beta} \|\mathbf{y} - \mathbf{x}\|^2, \quad (10)$$

where $\beta \in (0, \min\{\sigma^{-1}, \eta^{-1}\})$. Suppose that F admits a \mathcal{C}^3 -composite active manifold \mathcal{M} as defined in Definition 3.1 and that h is \mathcal{C}^4 -smooth near \mathbf{x}^* .¹ Then:

- (i) *H is \mathcal{C}^2 -smooth, and both H and ∇H are Lipschitz continuous around \mathbf{x}^* .*
- (ii) *Under Assumption A1, if the initial point \mathbf{x}^0 is sufficiently close to \mathbf{x}^* , then applying Anderson acceleration to (10) according to Algorithm 1 results in iterates that converge to \mathbf{x}^* R-linearly with $\hat{\gamma} \in (\gamma, 1)$; that is, (3) holds.*

Proof. The proximal linear algorithm has been shown to possess the active manifold identification property [23, Theorem 4.11]. Thus, the inclusions [10, Theorem 5.3] $H(\mathbf{x}) \in \mathcal{G}$ and $h(\mathbf{x}) + \nabla h(\mathbf{x})(H(\mathbf{x}) - \mathbf{x}) \in \mathcal{F}$ hold for all \mathbf{x} near \mathbf{x}^* . We can establish the smoothness of H

¹To apply the sensitivity analysis theory for establishing the \mathcal{C}^2 -smoothness of H , higher-order smoothness of h is required to ensure that the functions in (11) are \mathcal{C}^3 -smooth.

through sensitivity analysis. Consider any \mathcal{C}^3 -smooth functions $\hat{f} : \mathbb{R}^d \rightarrow \mathbb{R}$ and $\hat{g} : \mathbb{R}^n \rightarrow \mathbb{R}$ that agree with f and g near $h(\mathbf{x}^*)$ and \mathbf{x}^* on the smooth manifolds \mathcal{F} and \mathcal{G} . Then $H(\mathbf{x})$ solves the smooth problem near \mathbf{x}^* :

$$\begin{aligned} H(\mathbf{x}) = \arg \min_{\mathbf{y}} & \hat{f}(h(\mathbf{x}) + \nabla h(\mathbf{x})(\mathbf{y} - \mathbf{x})) + \hat{g}(\mathbf{y}) + \frac{1}{2\beta} \|\mathbf{y} - \mathbf{x}\|^2 \\ \text{s.t. } & \mathbf{y} \in \mathcal{G} \cap \mathcal{B}_{\mathbf{x}^*}(\hat{\rho}), \quad h(\mathbf{x}) + \nabla h(\mathbf{x})(\mathbf{y} - \mathbf{x}) \in \mathcal{F} \cap \mathcal{B}_{h(\mathbf{x}^*)}(\hat{\rho}), \end{aligned} \quad (11)$$

where $\mathcal{B}_{\mathbf{x}^*}(\hat{\rho})$ and $\mathcal{B}_{h(\mathbf{x}^*)}(\hat{\rho})$ are neighborhoods of \mathbf{x}^* and $h(\mathbf{x}^*)$ with radius $0 < \hat{\rho} \leq \rho$. By Definition 2.1, there exist mappings $G^{\mathcal{G}}$ and $G^{\mathcal{F}}$ that identify the locally defined equations of \mathcal{G} and \mathcal{F} . Thus, problem (11) can be reformulated as:

$$\zeta(\mathbf{x}) := H(\mathbf{x}), \quad v(\mathbf{x}, \mathbf{y}) := \hat{f}(h(\mathbf{x}) + \nabla h(\mathbf{x})(\mathbf{y} - \mathbf{x})) + \hat{g}(\mathbf{y}) + \frac{1}{2\beta} \|\mathbf{y} - \mathbf{x}\|^2,$$

where the constraints

$$\mathbf{y} \in \mathcal{G} \cap \mathcal{B}_{\mathbf{x}^*}(\hat{\rho}) \quad \text{and} \quad h(\mathbf{x}) + \nabla h(\mathbf{x})(\mathbf{y} - \mathbf{x}) \in \mathcal{F} \cap \mathcal{B}_{h(\mathbf{x}^*)}(\hat{\rho})$$

are equivalent to the condition $\{\mathbf{x} \in \mathbb{R}^n : G(\mathbf{x}, \mathbf{y}) = \mathbf{0}, J(\mathbf{x}, \mathbf{y}) \leq \mathbf{0}\}$ with

$$\begin{aligned} G(\mathbf{x}, \mathbf{y}) &:= \begin{bmatrix} G^{\mathcal{G}}(\mathbf{y}) \\ G^{\mathcal{F}}(h(\mathbf{x}) + \nabla h(\mathbf{x})(\mathbf{y} - \mathbf{x})) \end{bmatrix}, \\ J(\mathbf{x}, \mathbf{y}) &:= \begin{bmatrix} \|\mathbf{y} - \mathbf{x}^*\|^2 - \rho^2 \\ \|h(\mathbf{x}) + \nabla h(\mathbf{x})(\mathbf{y} - \mathbf{x}) - h(\mathbf{x}^*)\|^2 - \rho^2 \end{bmatrix}. \end{aligned}$$

To apply Lemma 2.2, we first verify its assumptions. The continuity of ζ is ensured by Lemma 2.1 under the condition $\beta \in (0, \min\{\sigma^{-1}, \eta^{-1}\})$, which implies that $\zeta(\mathbf{x}^*)$ is a strong global minimizer. The properties of the active manifolds \mathcal{G} and \mathcal{F} and the transversality condition (9) guarantee that the Jacobian $\nabla_{\mathbf{y}} G$ has full row rank at $(\mathbf{x}^*, \zeta(\mathbf{x}^*))$. Furthermore, the inequality constraint J is naturally inactive at $(\mathbf{x}^*, \zeta(\mathbf{x}^*))$. By applying Lemma 2.2, we conclude that H is \mathcal{C}^2 -smooth around \mathbf{x}^* . Similar to the analysis in Theorem 2, we complete the proof. \square

Remark There has been research on saddle point problems that demonstrates the smoothness of the mapping H as defined in (10). More details can be found in [10, Theorem 5.1]. Moreover, it is worth noting that Theorem 3 is also applicable to PPA and PGA with their corresponding simplified problems (as shown in Table 3). Furthermore, Definition 3.1 regarding composite active manifold reduces to Definition 2.2 in the context of PPA and PGA, with the non-degeneracy condition $\mathbf{0} \in \text{rint}(\partial F(\mathbf{x}^*))$.

4 Anderson-accelerated proximal coordinate descent algorithm

Consider the problem:

$$\min_{\mathbf{x} \in \mathbb{R}^n} F(\mathbf{x}) := f(\mathbf{x}) + \sum_{i=1}^n g_i(x_i), \quad (12)$$

where $f : \mathbb{R}^n \rightarrow \mathbb{R}$ is a \mathcal{C}^2 -smooth convex function with L_f -Lipschitz continuous gradients, and $g_i : \mathbb{R} \rightarrow \mathbb{R} \cup \{\infty\}, i = 1, \dots, n$ are proper, closed and convex. A common algorithm for solving such problems is the proximal coordinate descent algorithm (PCD) [15, 39]. In this paper, we focus on PCD in a cyclic scheme, which selects coordinate indices cyclically from

the set $\{1, \dots, n\}$. The iteration can be expressed as follows:

$$\begin{cases} \mathbf{x}^{k,1} &= \mathbf{x}^k + (\text{prox}_{\beta g_1}(x_1^k - \beta \nabla_1 f(\mathbf{x}^k)) - x_1^k) e_1, \\ \vdots & \\ \mathbf{x}^{k+1} &= \mathbf{x}^{k,n-1} + (\text{prox}_{\beta g_n}(x_n^{k,n-1} - \beta \nabla_n f(\mathbf{x}^{k,n-1})) - x_n^{k,n-1}) e_n, \end{cases} \quad (13)$$

Introduce $\psi_j : \mathbb{R}^n \rightarrow \mathbb{R}^n$ with the i th component defined by

$$[\psi_j(\mathbf{x})]_i := \begin{cases} \text{prox}_{\beta g_i}(x_i - \beta \nabla_i f(\mathbf{x})) & i = j, \\ x_i & i \neq j, \end{cases} \quad (14)$$

where $i, j = 1, \dots, n$. Given a fixed constant $\beta \in (0, L_f^{-1})$, (13) can be interpreted as a fixed-point iteration:

$$\mathbf{x}^{k+1} = H(\mathbf{x}^k) := \psi_n \circ \dots \circ \psi_1(\mathbf{x}^k) = \begin{bmatrix} [\psi_1(\mathbf{x}^k)]_1 \\ [(\psi_2 \circ \psi_1)(\mathbf{x}^k)]_2 \\ \dots \\ [(\psi_n \circ \dots \circ \psi_1)(\mathbf{x}^k)]_n \end{bmatrix}. \quad (15)$$

We also demonstrate the smoothness of the mapping H around \mathbf{x}^* through the active manifold identification property and Lemma 2.2, and establish the locally R-linear convergence rate of Anderson-accelerated PCD.

Theorem 4. *Consider the optimization problem (12). Let \mathbf{x}^* be a critical point of F and $H = \psi_n \circ \dots \circ \psi_1$ with $\beta \in (0, L_f^{-1})$. Suppose that g admits a C^3 -active manifold \mathcal{M} at \mathbf{x}^* , f is C^4 -smooth near \mathbf{x}^* , and $\mathbf{0} \in \text{rint}(\partial F(\mathbf{x}^*))$, then:*

- (i) H is C^2 -smooth, and both H and ∇H are Lipschitz continuous around \mathbf{x}^* .
- (ii) Under Assumption A1, if the initial point \mathbf{x}^0 is sufficiently close to \mathbf{x}^* , applying Anderson acceleration to (15) according to Algorithm 1 leads to iterates that converge to \mathbf{x}^* R-linearly with $\hat{\gamma} \in (\gamma, 1)$, i.e., (3) holds.

Proof. Given that F admits the active manifold \mathcal{M} , previous research has established the active manifold identification property of PCD [20]. Specifically, we have $H(\mathbf{x}) \in \mathcal{M}$ for all \mathbf{x} near \mathbf{x}^* . However, we cannot directly establish the smoothness of H through Lemma 2.2, as the mapping H does not correspond to a strongly convex function $s(\mathbf{x}, \cdot)$. Instead, we will infer the smoothness of H by analyzing the smoothness of $\psi := \psi_n \circ \dots \circ \psi_1$.

Let $\tilde{g} := \sum_{i=1}^n \tilde{g}_i$ with \tilde{g}_i being C^3 -smooth and coinciding with g_i for $i = 1, \dots, n$ on \mathcal{M} near \mathbf{x}^* . Consequently, the component $[\psi_1(\mathbf{x})]_1$ uniquely solves the following optimization problem:

$$\min_{y_1, \mathbf{y} \in \mathcal{M} \cap \mathcal{B}_{\mathbf{x}^*}(\hat{\rho})} s(\mathbf{x}, y_1) := \nabla_1 f(\mathbf{x}) y_1 + \tilde{g}_1(y_1) + \frac{1}{2\beta} (y_1 - x_1)^2,$$

where $\mathcal{B}_{\mathbf{x}^*}(\hat{\rho})$ is a neighborhood of \mathbf{x}^* with radius $0 < \hat{\rho} \leq \rho$. Given any $\mathbf{x} \in \mathbb{R}^n$, $s(\mathbf{x}, y_1)$ is strongly convex with respect to y_1 . Moreover, Lemma 2.1 implies that ψ is continuous. Thus, similar to the proof in Theorem 2, we can apply Lemma 2.2 to conclude that ψ_1 is C^2 -smooth around \mathbf{x}^* .

Similarly, the component $[(\psi_2 \circ \psi_1)(\mathbf{x})]_2$ uniquely solves the problem:

$$\min_{y_2, \mathbf{y} \in \mathcal{M} \cap \mathcal{B}_{\mathbf{x}^*}(\hat{\rho})} \nabla_2 f(\psi_1(\mathbf{x})) y_2 + \tilde{g}_2(y_2) + \frac{1}{2\beta} (y_2 - x_2)^2.$$

By applying Lemma 2.2, we derive that $[(\psi_2 \circ \psi_1)(\cdot)]_2$ is also \mathcal{C}^2 -smooth. Repeating this process, we obtain that $[(\psi_n \circ \dots \circ \psi_1)(\cdot)]_n$ is smooth, thus H is \mathcal{C}^2 -smooth around \mathbf{x}^* . Similar to the analysis in Theorem 2, statement (ii) can be proved. \square

5 Anderson-accelerated DRS/ADMM

We now consider the problem:

$$\min_{\mathbf{x} \in \mathbb{R}^n} F(\mathbf{x}) := f(\mathbf{x}) + g(\mathbf{x}), \quad (16)$$

where $f : \mathbb{R}^n \rightarrow \mathbb{R}$ is \mathcal{C}^2 -smooth with L_f -Lipschitz continuous gradients, and $g : \mathbb{R}^n \rightarrow \mathbb{R} \cup \{\infty\}$ is closed and σ -weakly convex. The Douglas-Rachford splitting algorithm (DRS) [17, 34] is a well-known method for solving such problems. Given $\mathbf{z}^0 \in \mathbb{R}^n$, $\beta \in (0, \min\{\sigma^{-1}, L_f^{-1}\})$, and $\delta \in (0, 2)$, the iteration of DRS is performed as follows:

$$\begin{cases} \mathbf{x}^{k+1} &= \text{prox}_{\beta f}(\mathbf{z}^k), \\ \mathbf{y}^{k+1} &= \text{prox}_{\beta g}(2\mathbf{x}^{k+1} - \mathbf{z}^k), \\ \mathbf{z}^{k+1} &= \mathbf{z}^k + \delta(\mathbf{y}^{k+1} - \mathbf{x}^k). \end{cases}$$

Introduce the mappings $R_\beta : \mathbb{R}^n \rightarrow \mathbb{R}$ and $S_\beta : \mathbb{R}^n \rightarrow \mathbb{R}$ defined by

$$R_\beta(\mathbf{z}) = \text{prox}_{\beta g}(2\text{prox}_{\beta f}(\mathbf{z}) - \mathbf{z}), \quad S_\beta(\mathbf{z}) = \mathbf{z} + \delta(R_\beta(\mathbf{z}) - \text{prox}_{\beta f}(\mathbf{z})).$$

It is worth noting that $R_\beta(\mathbf{z})$ is the solution to the DR envelope (DRE) [34] at \mathbf{z} :

$$\min_{\mathbf{y} \in \mathbb{R}^n} \langle \nabla f(\mathbf{x}(\mathbf{z})), \mathbf{y} - \mathbf{x}(\mathbf{z}) \rangle + g(\mathbf{y}) + \frac{1}{2\beta} \|\mathbf{y} - \mathbf{x}(\mathbf{z})\|^2, \quad (17)$$

where $\mathbf{x}(\mathbf{z}) = \text{prox}_{\beta f}(\mathbf{z})$. The DRS update (5) can be viewed as a fixed-point iteration: $\mathbf{z}^{k+1} = S_\beta(\mathbf{z}^k)$. Let \mathbf{z}^* be the fixed point of S_β . Then, the critical point \mathbf{x}^* of problem (16) and \mathbf{z}^* satisfy the following relations [1, Proposition 3]:

$$\mathbf{x}^* = \text{prox}_{\beta f}(\mathbf{z}^*) \quad \text{and} \quad -\nabla f(\mathbf{x}^*) \in \partial g(\mathbf{x}^*) \Leftrightarrow \mathbf{z}^* = S_\beta(\mathbf{z}^*).$$

Similarly, we can ensure the smoothness of the mapping $S_\beta(\mathbf{z})$ around \mathbf{z}^* with the help of the active manifold identification property and Lemma 2.2. We then establish the locally R-linear convergence rate of the Anderson-accelerated DRS algorithm.

Theorem 5. *Consider the optimization problem (16). Let \mathbf{x}^* be a critical point of F and \mathbf{z}^* a fixed point of $H(\mathbf{z})$ with $\beta \in (0, \min\{\sigma^{-1}, L_f^{-1}\})$. If g admits a C^3 -active manifold \mathcal{M} at \mathbf{x}^* , f is \mathcal{C}^4 -smooth near \mathbf{x}^* , and $\mathbf{0} \in \text{rint}(\partial F(\mathbf{x}^*))$, then:*

- (i) H is \mathcal{C}^2 -smooth; both H and ∇H are Lipschitz continuous around \mathbf{z}^* .
- (ii) Under Assumption A1, if the initial point \mathbf{x}^0 is sufficiently close to \mathbf{x}^* , then applying Anderson acceleration to $\mathbf{z} = H(\mathbf{z}) := S_\beta(\mathbf{z})$ according to Algorithm 1 leads to convergence of the generated iterates to \mathbf{z}^* R-linearly with $\hat{\gamma} \in (\gamma, 1)$; i.e. (3) holds.

Proof. Research has established the active manifold identification property and the local smoothness of H . For completeness, we briefly summarize these results; additional details can be found in [1, Theorem 2]. In the context of the DRS algorithm, the active manifold identification property manifests as follows: For all \mathbf{z} near \mathbf{z}^* , we have $\mathbf{y} = R_\beta(\mathbf{z}) \in \mathcal{M}$. By applying Lemma 2.2 to the DRE as defined in (17), with the condition $\beta \in (0, \min\{\sigma^{-1}, L_f^{-1}\})$,

we deduce that R_β is \mathcal{C}^2 -smooth around \mathbf{z}^* . Consequently, this implies the \mathcal{C}^2 -smoothness of S_β . Following a similar argument as in Theorem 2, we conclude the proof. \square

Remark Given the established equivalence between DRS and ADMM [13, 34], our analysis also applies to Anderson-accelerated ADMM. We consider the following linearly constrained optimization problem:

$$\min_{(\mathbf{u}, \mathbf{w}) \in \mathbb{R}^m \times \mathbb{R}^n} \varphi_1(\mathbf{u}) + \varphi_2(\mathbf{w}) \quad \text{s.t.} \quad A\mathbf{u} + B\mathbf{w} = \mathbf{b}, \quad (18)$$

where $\varphi_1 : \mathbb{R}^m \rightarrow \mathbb{R} \cup \{\infty\}$, $\varphi_2 : \mathbb{R}^n \rightarrow \mathbb{R} \cup \{\infty\}$, $A \in \mathbb{R}^{p \times m}$, $B \in \mathbb{R}^{p \times n}$ and $\mathbf{b} \in \mathbb{R}^p$. The iterative scheme of ADMM is described as follows:

$$\begin{cases} \mathbf{u}^{k+1} &= \arg \min L_\lambda(\cdot, \mathbf{w}^k, \mathbf{v}^k), \\ \mathbf{v}^{k+1} &= \mathbf{v}^k + \lambda(A\mathbf{u}^{k+1} + B\mathbf{w}^k - \mathbf{b}), \\ \mathbf{w}^{k+1} &= \arg \min L_\lambda(\mathbf{w}^{k+1}, \cdot, \mathbf{v}^{k+1}). \end{cases}$$

Here, $\lambda > 0$ is a penalty parameter, and the augmented Lagrangian L_λ is defined as:

$$L_\lambda(\mathbf{u}, \mathbf{w}, \mathbf{v}) := \varphi_1(\mathbf{u}) + \varphi_2(\mathbf{w}) + \langle \mathbf{v}, A\mathbf{u} + B\mathbf{w} - \mathbf{b} \rangle + \frac{\lambda}{2} \|A\mathbf{u} + B\mathbf{w} - \mathbf{b}\|^2.$$

For nonconvex problems, [34] thoroughly analyzes the equivalence between ADMM and DRS using the notion of the *image function*. Through a primal reformulation, it is shown that ADMM for (18) is essentially equivalent to applying DRS to (16) with $f = (A\varphi_1)$ and $g = (B\varphi_2)(\mathbf{b} - \cdot)$. For a detailed explanation, readers are encouraged to refer to [34, Section 5.1]. The correspondence between DRS variables $(\mathbf{x}, \mathbf{y}, \mathbf{z})$ and ADMM variables $(\mathbf{u}, \mathbf{v}, \mathbf{w})$ is established in [34, Theorem 5.5] as follows:

$$\mathbf{x} = A\mathbf{u}, \quad \mathbf{y} = \mathbf{b} - B\mathbf{w}, \quad \mathbf{z} = A\mathbf{u} - \mathbf{v}/\lambda. \quad (19)$$

We now proceed to establish the local smoothness of the ADMM mapping $(\mathbf{u}^k, \mathbf{v}^k, \mathbf{w}^k)$

$\xrightarrow{\text{ADMM}} (\mathbf{u}^{k+1}, \mathbf{v}^{k+1}, \mathbf{w}^{k+1})$ under the following two conditions:

- (i) Problem (16) with $f = (A\varphi_1)$ and $g = (B\varphi_2)(\mathbf{b} - \cdot)$ satisfies the assumptions in Theorem 5.
- (ii) The correspondence between DRS variables $(\mathbf{x}, \mathbf{y}, \mathbf{z})$ and ADMM variables $(\mathbf{u}, \mathbf{v}, \mathbf{w})$ is one-to-one, meaning $m = n = p$ and both A and B are invertible.

Under the first condition, Theorem 5 establishes the local smoothness of the mappings R_β and S_β , further demonstrating the local smoothness of the entire mapping $(\mathbf{x}^k, \mathbf{y}^k, \mathbf{z}^k) \xrightarrow{\text{DRS}} (\mathbf{x}^{k+1}, \mathbf{y}^{k+1}, \mathbf{z}^{k+1})$ as defined in (5). The second condition guarantees a one-to-one correspondence between $(\mathbf{x}, \mathbf{y}, \mathbf{z})$ and $(\mathbf{u}, \mathbf{v}, \mathbf{w})$, establishing that the mapping $(\mathbf{u}^k, \mathbf{v}^k, \mathbf{w}^k) \xrightarrow{\text{ADMM}} (\mathbf{u}^{k+1}, \mathbf{v}^{k+1}, \mathbf{w}^{k+1})$ is smooth. Using similar reasoning, we can also prove the local convergence rate of Anderson acceleration for $(\mathbf{u}^k, \mathbf{v}^k, \mathbf{w}^k) \xrightarrow{\text{ADMM}} (\mathbf{u}^{k+1}, \mathbf{v}^{k+1}, \mathbf{w}^{k+1})$.

6 Anderson-accelerated iteratively reweighted ℓ_1 algorithm

In the previous sections, we established the local smoothness of iteration mappings for various algorithms within the context of weakly convex nonsmooth functions. In this section, we shift our focus to a class of nonconvex regularized optimization problems and the corresponding algorithm, the iteratively reweighted ℓ_1 algorithm (IRL1) [18, 26]. We will demonstrate the

local smoothness of the iteration mapping of IRL1 and confirm the local linear convergence rate of Anderson acceleration for this algorithm.

Consider the following nonconvex regularized optimization problem:

$$\min_{\mathbf{x} \in \mathbb{R}^n} F(\mathbf{x}) := f(\mathbf{x}) + \lambda \sum_{i=1}^n \phi(|x_i|), \quad (20)$$

where $f : \mathbb{R}^n \rightarrow \mathbb{R}$ is Lipschitz continuously differentiable, $\lambda > 0$, and $\phi : \mathbb{R}_+ \rightarrow \mathbb{R}_+$ is a nonsmooth regularization function. The function ϕ takes various forms, such as the EXP approximation [6], LPN approximation [14], LOG approximation [25], FRA approximation [14], and TAN approximation [7]. Table 4 presents the explicit forms for these cases. p is a hyperparameter that controls sparsity. In this section, we impose the following assumptions on F defined in (20).

| | EXP [6] | LPN [14] | LOG [25] | FRA [14] | TAN [7] |
|---------------|-------------------|-----------|--------------------|-------------------------|-------------------|
| p | $(0, +\infty)$ | $(0, 1)$ | $(0, +\infty)$ | $(0, +\infty)$ | $(0, +\infty)$ |
| $\phi(x_i)$ | $1 - e^{-p x_i }$ | $ x_i ^p$ | $\log(1 + p x_i)$ | $\frac{ x_i }{ x_i +p}$ | $\arctan(p x_i)$ |

Table 4: Different functions $\phi(|x_i|)$

Assumption A2. (i) f has L_f -Lipschitz continuous gradients.

(ii) ϕ is smooth, concave, and strictly increasing on $(0, +\infty)$, with $\phi(0) = 0$.

(iii) F is non-degenerate in the sense that for any critical point \mathbf{x}^* of F , it holds that $\mathbf{0} \in \text{rint } \partial F(\mathbf{x}^*)$.

For problem (20), we provide a more intuitive derivation using non-degeneracy conditions to demonstrate that IRL1 possesses the property of active manifold identification. For the LPN approximation, the non-degeneracy condition naturally holds because $\lambda\phi'(0^+) = \lambda p(0^+)^{p-1} = \infty$, which significantly dominates $\nabla_i f(0^+)$ in the optimality condition. For other sparse approximations, the values of λ and p are typically adjusted to ensure sparsity, which requires either λ or $\phi'(0^+)$ to be sufficiently large to satisfy the non-degeneracy condition.

To address the nonsmoothness of the objective function in (20), a common technique in IRL1 involves adding a perturbation vector $\boldsymbol{\epsilon} \in \mathbb{R}_+^n$, leading to a continuously differentiable function:

$$F(\mathbf{x}, \boldsymbol{\epsilon}) := f(\mathbf{x}) + \lambda \sum_{i=1}^n \phi(|x_i| + \epsilon_i).$$

Under Assumption A2, for any $\beta \in (0, L_f^{-1})$ and for any \mathbf{x} near \mathbf{x}^k , the following holds:

$$F(\mathbf{x}, \boldsymbol{\epsilon}) \leq f(\mathbf{x}^k) + \nabla f(\mathbf{x}^k)^T (\mathbf{x} - \mathbf{x}^k) + \frac{1}{2\beta} \|\mathbf{x} - \mathbf{x}^k\|_2^2 + \lambda \sum_{i=1}^n \phi'(|x_i^k| + \epsilon_i^k) (|x_i| - |x_i^k|).$$

Consequently, in the k -th iteration of IRL1, a convex subproblem that locally approximates F is solved to obtain the new iterate \mathbf{x}^{k+1} :

$$\mathbf{x}^{k+1} = \arg \min_{\mathbf{x} \in \mathbb{R}^n} G_k(\mathbf{x}) := Q_k(\mathbf{x}) + \lambda \sum_{i=1}^n \omega_i^k |x_i|, \quad (21)$$

where $\omega_i^k := \phi'(|x_i^k| + \epsilon_i^k)$ and $Q_k(\mathbf{x}) := \nabla f(\mathbf{x}^k)^T \mathbf{x} + \frac{1}{2\beta} \|\mathbf{x} - \mathbf{x}^k\|^2$. The subproblem (21) has a closed-form solution:

$$x_i^{k+1} = \begin{cases} x_i^k - \beta \nabla_i f(\mathbf{x}^k) + \beta \lambda \omega_i^k & \text{if } x_i^k - \beta \nabla_i f(\mathbf{x}^k) < -\beta \lambda \omega_i^k, \\ x_i^k - \beta \nabla_i f(\mathbf{x}^k) - \beta \lambda \omega_i^k & \text{if } x_i^k - \beta \nabla_i f(\mathbf{x}^k) > \beta \lambda \omega_i^k, \\ 0 & \text{otherwise.} \end{cases} \quad (22)$$

In the IRL1 algorithm, the choice of ϵ significantly impacts performance. Large ϵ smoothes out overlook many local minimizers. while small ϵ make the subproblem difficult to solve due to bad minimizers. A common strategy is to initialize the algorithm with a relatively large ϵ^0 and drive it toward 0 during successive iterations. Dynamic update schemes for ϵ have been proposed by Wang et al. [38] and Lu [26].

In this paper, we adopt the update scheme proposed by these authors:

$$\epsilon^{k+1} = \mu \epsilon^k \quad (23)$$

in IRL1, where $\mu \in (0, 1)$ controls the decay rate. By introducing

$$\boldsymbol{\theta} := \begin{bmatrix} \mathbf{x} \\ \epsilon \end{bmatrix} \quad \text{and} \quad H : \mathbb{R}^{2n} \rightarrow \mathbb{R}^{2n} \text{ defined as } H(\boldsymbol{\theta}) := \begin{bmatrix} \arg \min_{\mathbf{y} \in \mathbb{R}^n} G_k(\mathbf{y}) \\ \mu \epsilon \end{bmatrix}, \quad (24)$$

we can represent the iteration of IRL1, i.e. (21) and (23), as a fixed-point iteration $\boldsymbol{\theta}^{k+1} = H(\boldsymbol{\theta}^k)$. Denote $\boldsymbol{\theta}^* = [\mathbf{x}^*; \mathbf{0}]$. For simplicity, we introduce $H(\boldsymbol{\theta}) = [H_1(\boldsymbol{\theta}); H_2(\boldsymbol{\theta})]$ with mappings $H_1 : \mathbb{R}^{2n} \rightarrow \mathbb{R}^n$ and $H_2 : \mathbb{R}^{2n} \rightarrow \mathbb{R}^n$ defined by

$$H_1(\boldsymbol{\theta}) = \arg \min_{\mathbf{y} \in \mathbb{R}^n} G_k(\mathbf{y}), \quad H_2(\boldsymbol{\theta}) = \mu \epsilon.$$

We proceed to analyze the local smoothness of H . Denote $\mathcal{A}^* := \{i \mid x_i^* = 0\}$ and $\mathcal{I}^* := \{i \mid x_i^* \neq 0\}$. A notable property of IRL1 for (20) is the locally stable sign property of the iterates $\{\mathbf{x}^k\}$, meaning that $\text{sign}(\mathbf{x}^k)$ remains unchanged for sufficiently large k [38]. Towards the end of the iteration, IRL1 is equivalent to solving a smooth problem in the reduced space $\mathbb{R}^{\mathcal{I}^*}$, a property known as model identification. We generalize this concept to the general nonconvex regularized problem (20) by leveraging the active manifold identification property, which can be established based on the non-degeneracy condition required by Assumption A2. We then infer the local smoothness of H .

Lemma 6.1 (Active manifold identification and local smoothness). *Let Assumption A2 hold. There exists a neighborhood $\mathcal{B}_{\boldsymbol{\theta}^*}(\rho)$ of $\boldsymbol{\theta}^*$ such that for all $\boldsymbol{\theta} \in \mathcal{B}_{\boldsymbol{\theta}^*}(\rho)$, the following statements hold:*

- (i) $H(\boldsymbol{\theta}) \in \mathcal{M}$, where $\mathcal{M} := \{\boldsymbol{\theta} = [\mathbf{x}; \epsilon] \mid \text{sign}(\mathbf{x}) = \text{sign}(\mathbf{x}^*), \epsilon \in \mathbb{R}_+^n\}$.
- (ii) $H(\boldsymbol{\theta})$ is continuously differentiable.

Proof. (i) It is straightforward to observe that $H_2(\boldsymbol{\theta}) = \mu \epsilon \in \mathbb{R}_+^n$.

To prove that $\text{sign}(H_1(\boldsymbol{\theta})) = \text{sign}(\mathbf{x}^*)$, consider $i \in \mathcal{A}^*$. The non-degeneracy condition $-\nabla_i f(\mathbf{x}^*) \in \text{rint}(\lambda \partial \phi(x_i^*))$ and the symmetry of ϕ imply that $|\nabla_i f(\mathbf{x}^*)| < |\lambda \omega(\theta_i^*)|$. Since $x_i^* = 0$, we have $|x_i^* - \beta \nabla_i f(\mathbf{x}^*)| < |\beta \lambda \omega(\theta_i^*)|$. Combining this with the continuity of F , we deduce that there exists a sufficiently small constant $\rho > 0$ such that for all $\boldsymbol{\theta} \in \mathcal{B}_{\boldsymbol{\theta}^*}(\rho)$, $|x_i - \beta \nabla_i f(\mathbf{x})| < |\beta \lambda \omega(\theta_i)|$. Therefore, $[H_1(\boldsymbol{\theta})]_i = 0$, which is also evident from (22). Then we deduce that $\text{sign}([H_1(\boldsymbol{\theta})]_i) = \text{sign}(x_i^*)$. For $i \in \mathcal{I}^*$, the continuity of H implies that there exists a sufficiently small constant $\rho > 0$ such that for all $\boldsymbol{\theta} \in \mathcal{B}_{\boldsymbol{\theta}^*}(\rho)$, it holds that $\text{sign}(x_i) = \text{sign}(x_i^*)$ and $\text{sign}([H_1(\boldsymbol{\theta})]_i) = \text{sign}(x_i^*)$.

(ii) Given $\boldsymbol{\theta} \in \mathcal{B}_{\boldsymbol{\theta}^*}(\rho)$ and $\text{sign}([H(\boldsymbol{\theta})]_i) = \text{sign}(x_i^*)$, it follows that $H(\boldsymbol{\theta})$ is continuously differentiable in $\mathcal{B}_{\boldsymbol{\theta}^*}(\rho)$. \square

In the context of IRL1, we provide a specific analysis demonstrating that H is both a contraction and Lipschitz continuously differentiable. Let $\Phi := \sum_{i=1}^n \phi$. We introduce the following assumption for the subsequent analysis.

Assumption A3. Let $\boldsymbol{\theta}^* = [\mathbf{x}^*; 0]$ be the fixed point of H , and let $\mathcal{B}_{\boldsymbol{\theta}^*}(\rho)$ denote a neighborhood around $\boldsymbol{\theta}^*$. For all $\boldsymbol{\theta} \in \mathcal{B}_{\boldsymbol{\theta}^*}(\rho)$, the following conditions hold:

- (i) $[\nabla_{\mathbf{x}\mathbf{x}}^2 F(\boldsymbol{\theta})]_{\mathcal{I}^*} \succeq \kappa I$ for some $\kappa > 0$, and $[\nabla_{\mathbf{x}\mathbf{x}}^2 F(\boldsymbol{\theta})]_{\mathcal{I}^*}$ is Lipschitz continuous.
- (ii) $[\nabla_{\mathbf{x}\boldsymbol{\epsilon}}^2 \Phi(\boldsymbol{\theta})]_{\mathcal{I}^*}$ is Lipschitz continuous with a constant $L_w > 0$.

In the following theorem, we show that $H(\boldsymbol{\theta})$ is a contraction and Lipschitz continuously differentiable when $\boldsymbol{\theta}$ is near $\boldsymbol{\theta}^*$, and we establish the local convergence rate of the Anderson-accelerated IRL1.

Theorem 6. Consider the problem (20). Let Assumptions A2 and A3 hold, \mathbf{x}^* be a critical point of F , and H be defined in (24) with $\mu \in (0, 1 - \sqrt{\lambda^2 L_\omega^2 / (\kappa^2 + \lambda^2 L_\omega^2)})$ and $\beta \in (\underline{\beta}, \bar{\beta})$, where $\underline{\beta}, \bar{\beta}$ are the two roots of

$$(\kappa^2 + \lambda^2 L_\omega^2)\beta^2 - 2\kappa\beta + 2\mu - \mu^2 = 0. \quad (25)$$

Then the following statements hold:

- (i) $H(\boldsymbol{\theta})$ is Lipschitz continuously differentiable and a contraction for all $\boldsymbol{\theta} \in \mathcal{B}_{\boldsymbol{\theta}^*}(\rho)$, i.e., there exists $\gamma \in (0, 1)$ such that

$$\|H(\boldsymbol{\theta}_1) - H(\boldsymbol{\theta}_2)\| \leq \gamma \|\boldsymbol{\theta}_1 - \boldsymbol{\theta}_2\|, \quad \forall \boldsymbol{\theta}_1, \boldsymbol{\theta}_2 \in \mathcal{B}_{\boldsymbol{\theta}^*}(\rho). \quad (26)$$

- (ii) If the initial point $\boldsymbol{\theta}^0$ is sufficiently close to $\boldsymbol{\theta}^*$ and Assumption A1(ii) holds, when applying Anderson acceleration to H defined in (24) following Algorithm 1, the generated iterates converge to $\boldsymbol{\theta}^*$ R -linearly with $\hat{\gamma} \in (\gamma, 1)$, i.e., (3) holds.

Proof. (i) First, we can derive that

$$\nabla H = \left[\begin{array}{c|c} [\nabla_{\mathbf{x}} H_1]_{\mathcal{I}^*} & \nabla_{\mathbf{x}} H_2 \\ \hline [\nabla_{\mathbf{x}} H_1]_{\mathcal{A}^*} & \nabla_{\mathbf{x}} H_2 \end{array} \right]^T = \left[\begin{array}{c|c} I - \beta[\nabla_{\mathbf{x}\mathbf{x}}^2 F]_{\mathcal{I}^*} & 0 \\ \hline 0 & 0 \\ -\beta\lambda[\nabla_{\mathbf{x}\boldsymbol{\epsilon}}^2 \Phi]_{\mathcal{I}^*} & \mu I \\ \hline 0 & \mu I \end{array} \right]^T. \quad (27)$$

From the Lipschitz continuity of $[\nabla_{\mathbf{x}\mathbf{x}}^2 F]_{\mathcal{I}^*}$ and $[\nabla_{\mathbf{x}\boldsymbol{\epsilon}}^2 \Phi]_{\mathcal{I}^*}$ as stated in Assumption A3, we can deduce that ∇H is Lipschitz continuous. Additionally, with $\|[\nabla_{\mathbf{x}\mathbf{x}}^2 F]_{\mathcal{I}^*}\| \geq \kappa$ and $\|[\nabla_{\mathbf{x}\boldsymbol{\epsilon}}^2 \Phi]_{\mathcal{I}^*}\| \leq L_w$, we further obtain

$$\|\nabla_{\mathbf{x}} H_1\| \leq 1 - \beta\kappa \quad \text{and} \quad \|\nabla_{\boldsymbol{\epsilon}} H_1\| \leq \beta\lambda L_w. \quad (28)$$

From (27) we have

$$\begin{aligned} \|\nabla H\| &\leq \|\nabla H_1\| + \|\nabla H_2\| = \sqrt{\|\nabla H_1[\nabla H_1]^T\|} + \|\nabla H_2\| \\ &= \sqrt{\|\nabla_{\mathbf{x}} H_1[\nabla_{\mathbf{x}} H_1]^T + \nabla_{\boldsymbol{\epsilon}} H_1[\nabla_{\boldsymbol{\epsilon}} H_1]^T\|} + \|\nabla H_2\| \\ &\leq \sqrt{\|\nabla_{\mathbf{x}} H_1\|^2 + \|\nabla_{\boldsymbol{\epsilon}} H_1\|^2} + \|\nabla H_2\| \leq \sqrt{(1 - \beta\kappa)^2 + \beta^2\lambda^2 L_w^2} + \mu, \end{aligned} \quad (29)$$

where the first and second inequalities follow from the triangle inequality, and the third inequality follows from (28). Note that $\mu \in (0, 1 - \sqrt{\lambda^2 L_\omega^2 / (\kappa^2 + \lambda^2 L_\omega^2)})$ guarantees the existence of roots of (28). Combining $\beta \in (\underline{\beta}, \overline{\beta})$ and (25), we have

$$\sqrt{(1 - \beta\kappa)^2 + \beta^2 \lambda^2 L_\omega^2} + \mu < 1,$$

which, together with (29), implies that $\|\nabla H\| < 1$. That is, H is a contraction for all $\theta \in \mathcal{B}_{\theta^*}(\rho)$, and (26) holds.

(ii) With the contractivity and Lipschitz continuous differentiability of H , applying Theorem 1 enables us to establish the local convergence rate. \square

7 Numerical experiments

In this section, we demonstrate the performance of Anderson-accelerated nonsmooth optimization algorithms using several well-known examples from signal processing and machine learning. All experiments are implemented in MATLAB 2022a on a 64-bit laptop equipped with an Intel Core i7-1165G7 processor (2.80GHz) and 16GB of RAM. We conduct experiments using both synthetic and real-world datasets, with the initial point \mathbf{x}^0 drawn from a standard Gaussian distribution. For each experiment, we plot the residual norm $\|\mathbf{r}^k\|$ at each iteration k to validate our theoretical results. Since the additional computational cost of Anderson Acceleration (AA) per iteration is less than 10%, the runtime plots closely resemble the iteration count plots, we omit the runtime plots in the following experiments.

7.1 PGA for sparse signal recovery

We begin with the classic Lasso problem in signal processing [35]:

$$\min_{\mathbf{x} \in \mathbb{R}^N} F(\mathbf{x}) := \frac{1}{2} \|\mathbf{A}\mathbf{x} - \mathbf{y}\|^2 + \lambda \|\mathbf{x}\|_1,$$

where $A \in \mathbb{R}^{M \times N}$ and $\mathbf{y} \in \mathbb{R}^M$. The objective is to recover a sparse signal \mathbf{x} from M observations, with $M \ll N$. We compare the performance of classical ISTA, FISTA, and Anderson-accelerated ISTA (AAISTA). The entries of matrix A are generated randomly and independently from a standard Gaussian distribution, and A is orthonormalized along its rows. The true signal \mathbf{x}_{true} is created by randomly selecting $N/10$ elements from an N -dimensional zero vector and setting them to ± 1 . The observation vector is defined as $\mathbf{y} = \mathbf{A}\mathbf{x}_{\text{true}} + \boldsymbol{\epsilon}$, where $\boldsymbol{\epsilon} \in \mathbb{R}^N$ follows a Gaussian distribution with mean 0 and variance 10^{-4} . We set $\lambda = 0.01$ and $M = 15$. Figure 3 shows the average performance over 50 random experiments. It can be observed that the AAISTA curve exhibits a significant change toward the end of the iterations, transitioning from a sublinear to a linear, or even superlinear, convergence rate. This behavior suggests that active manifold identification has occurred, significantly accelerating the algorithm. This observation corroborates our theoretical predictions.

7.2 PCD, DRS, and IRL1 for classification problems

In this section, we compare the performance of the PCD, DRS, and IRL1 algorithms with their respective Anderson-accelerated versions—AAPCD, AADRS, and AAIRL1—across several classification models using five real-world datasets: *mushrooms*, *colon-cancer*, *ijcnn1*, *w8a*, and *a9a*. These datasets consist of binary classification problems from the LIBSVM repository [8]. A summary of the datasets is provided in Table 5. Let $\mathbf{a}_i \in \mathbb{R}^N$ denote the training samples,

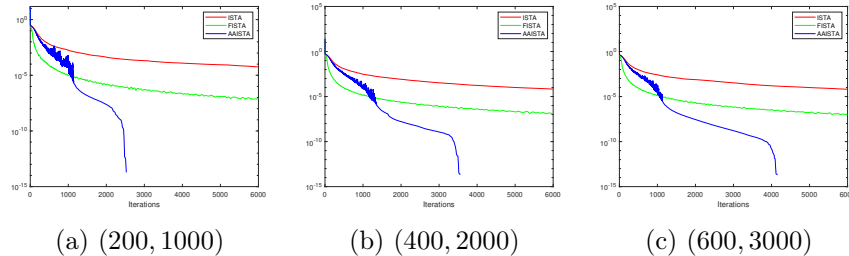


Figure 3: Comparison of $\|\mathbf{r}^k\|$ for ISTA, FISTA, AAISTA under different (M, N) .

and $A = [\mathbf{a}_1, \dots, \mathbf{a}_M]^T \in \mathbb{R}^{M \times N}$ represent the matrix of training samples, while $\mathbf{y} \in \{-1, 1\}^M$ denotes the corresponding labels. During the experiments, we observed instances of non-

| Datasets | mushrooms | colon-cancer | ijcnn1 | a9a | w8a |
|--------------|-----------|--------------|--------|-------|-------|
| Samples M | 8124 | 62 | 49990 | 32561 | 49749 |
| Features N | 112 | 2000 | 22 | 123 | 300 |

Table 5: Characteristics of the datasets

convergence when using Anderson Acceleration (abbreviated as AA). To ensure convergence, we incorporated a function/residual descent check to confirm that AA iterates converge to the desired local region. In each experiment, we tested three different memory sizes for AA, $m = 5, 10, 15$, denoted as AA(m). The results indicate that AA demonstrates significant effectiveness, particularly in local regions for real-world tasks. It is also noteworthy that the optimal memory size m may vary depending on the specific problem.

PCD for support vector machines In this subsection, we focus on the PCD method for solving the soft margin Support Vector Machine (SVM), which can be tackled through the following dual optimization problem:

$$\min_{\mathbf{x} \in \mathbb{R}^M} F(\mathbf{x}) := \frac{1}{2} \|(\mathbf{y} \odot A)^T \mathbf{x}\|^2 - \sum_{i=1}^M x_i \quad \text{s.t.} \quad 0 \leq \mathbf{x} \leq C,$$

where $\mathbf{y} \odot A$ denotes the element-wise multiplication between \mathbf{y} and A . This problem can be reformulated in the form (12) by defining $f(\mathbf{x}) = F(\mathbf{x})$ and $g_i(\mathbf{x}) = \chi_{[0, C]}(x_i)$ for $i = 1, \dots, M$. Soft margin SVM extends the traditional SVM by allowing some misclassifications, with the parameter C controlling the tolerance for misclassification. In our experiments, we set $C = 100$. The PCD update for this problem is given by: $x_i = \text{prox}_{\beta \chi_{[0, C]}}(x_i - \beta ((\mathbf{y} \odot A)(\mathbf{y} \odot A)^T)_{i,:} \mathbf{x} - 1)$, where $\beta = 1/L$ and $L = \max_{i=1, \dots, M} \|(\mathbf{y} \odot A)_{i,:}\|^2$. Given the large number of samples in these datasets, PCD requires a significant number of iterations to compute x_i for each sample. Thus, we randomly selected 2000 samples from each dataset: *mushrooms*, *ijcnn1*, *w8a*, and *a9a* for the experiments. Figure 4 compares the performance of AAPCD and the classical PCD algorithm. As shown, the AAPCD curve experiences a sharp decline in the final stages, perfectly aligning with our theoretical predictions. In some challenging experiments, the AA curve closely follows the standard algorithm during the initial iterations, indicating that the AA step is seldom activated early on, leading to an unaccelerated algorithm. This also highlights the global instability of the AA method.

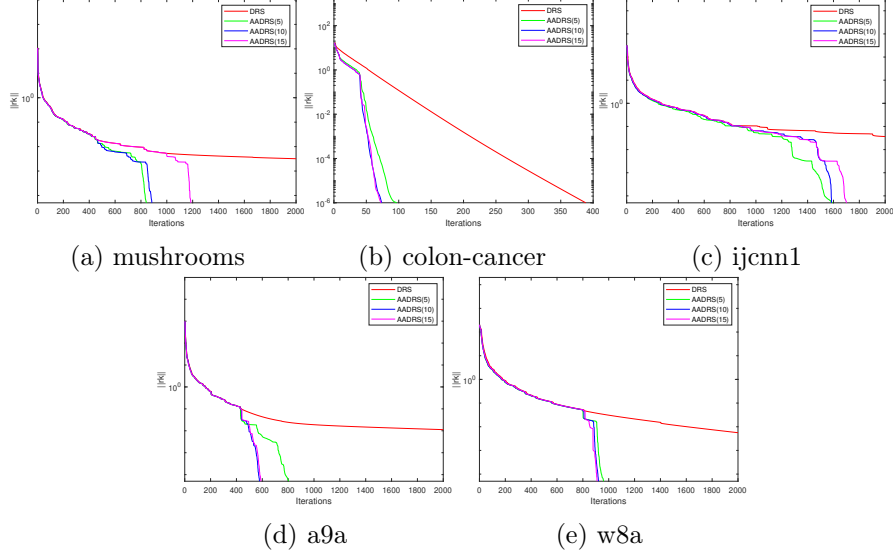


Figure 4: Comparison of $\|\mathbf{r}^k\|$ for PCD and AAPCD(m).

DRS for nonnegative least squares In this section, we explore the DRS method for solving the nonnegative least squares problem:

$$\min_{\mathbf{x} \in \mathbb{R}^N} F(\mathbf{x}) := \frac{1}{2M} \|\mathbf{A}\mathbf{x} - \mathbf{y}\|^2 + \lambda \|\mathbf{x}\|^2 \quad \text{s.t. } \mathbf{x} \geq 0,$$

which is a common step in many nonnegative matrix factorization algorithms. This problem can be reformulated as (16) by defining $f(\mathbf{x}) = F(\mathbf{x})$ and $g(\mathbf{x}) = \chi_{[0, +\infty]}(\mathbf{x})$. We set $\lambda = 0.001$ and $\beta = 1/L$, where $L = \|\mathbf{A}\|^2/M$. The computation of $\text{prox}_{\beta g}$ is straightforward and given by $\max(0, \mathbf{x})$. For $\text{prox}_{\beta f}$, it actually corresponds to a least-square problem, which we solve using LSQR, an efficient conjugate gradient method for sparse least-squares problems. Figure 5 shows the residual curves from our experiments. AA demonstrates significant acceleration. For instance, in Figure 5(c), AA quickly identifies a high-precision solution, especially when handling ill-conditioned datasets.

IRL1 for sparse logistic regression In this subsection, we report the results of using the IRL1 method to solve the sparse logistic regression problem:

$$\min_{\mathbf{x} \in \mathbb{R}^N} F(\mathbf{x}) := \frac{1}{M} \sum_{i=1}^M \log(1 + \exp(-y_i \mathbf{a}_i^T \mathbf{x})) + \lambda \|\mathbf{x}\|_p^p,$$

where we set $p = 0.75$, $\lambda = 0.001$, $\epsilon^0 = \mathbf{1}$, $\mu = 0.9$, and $\beta = 1/L$, with $L = \|\mathbf{A}\|^2/4M$. The results are presented in Figure 6. Anderson Acceleration provides a speedup of approximately 5-10 times, with most of the improvement occurring in the final stages of descent. In Figures 6 (a) and (e), it appears that AA identifies the solution in a finite number of steps, possibly because the solution lies in the subspace spanned by previous iterations.

8 Conclusions

In this paper, we have analyzed the local convergence rate of Anderson acceleration for nonsmooth optimization algorithms that exhibit the active manifold identification property. These algorithms include proximal point, proximal gradient, proximal linear, proximal coordinate de-

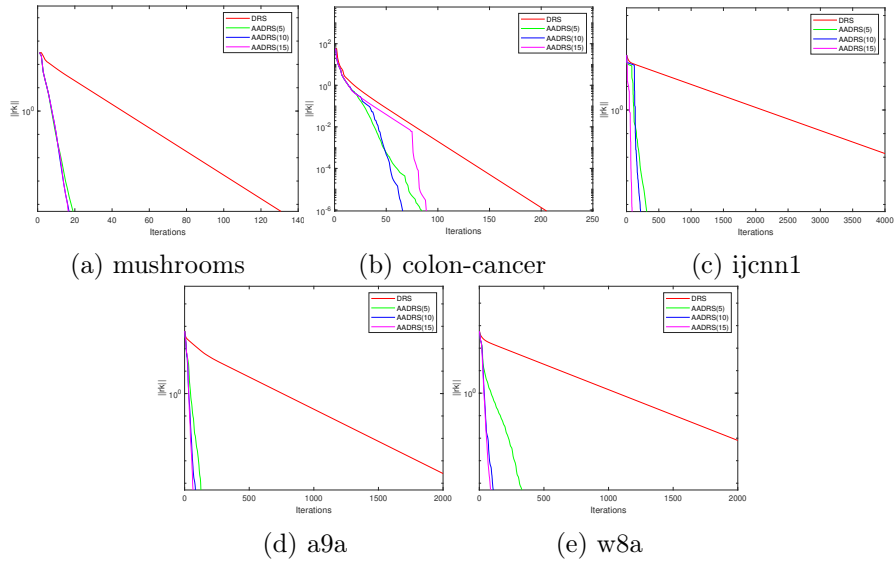


Figure 5: Comparison of $\|r^k\|$ for DRS and AADR(m).

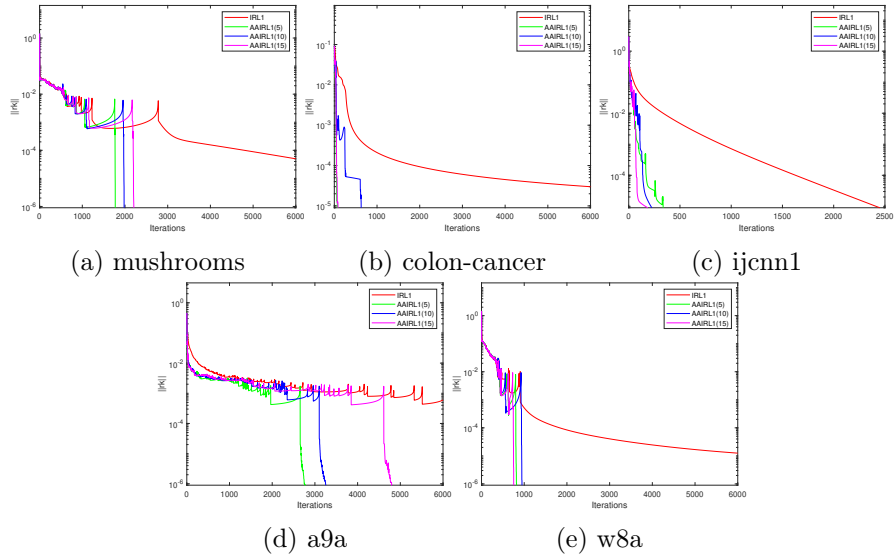


Figure 6: Comparison of $\|r^k\|$ for IRL1 and AAIRL1(m).

scent, Douglas-Rachford splitting/alternating direction method of multipliers and iteratively reweighted ℓ_1 algorithms, covering a broad range of nonsmooth optimization problems. Our work fills a gap in the convergence rate analysis of Anderson-accelerated nonsmooth optimization algorithms and provides a rigorous explanation for the effectiveness of Anderson acceleration when applied to these methods.

References

- [1] F. Atenas. Weakly convex douglas-rachford splitting avoids strict saddle points. *Optimization Online*, 2024.
- [2] A. Beck and M. Teboulle. A fast iterative shrinkage-thresholding algorithm for linear inverse problems. *SIAM Journal on Imaging Sciences*, 2(1):183–202, 2009.
- [3] Q. Bertrand and M. Massias. Anderson acceleration of coordinate descent. In *International Conference on Artificial Intelligence and Statistics*, pages 1288–1296. PMLR, 2021.
- [4] W. Bian and X. Chen. Anderson acceleration for nonsmooth fixed point problems. *SIAM Journal on Numerical Analysis*, 60(5):2565–2591, 2022.
- [5] W. Bian, X. Chen, and C. T. Kelley. Anderson acceleration for a class of nonsmooth fixed-point problems. *SIAM Journal on Scientific Computing*, 43(5):S1–S20, 2021.
- [6] P. S. Bradley, O. L. Mangasarian, and W. N. Street. Feature selection via mathematical programming. *INFORMS Journal on Computing*, 10(2):209–217, 1998.
- [7] E. J. Candes, M. B. Wakin, and S. P. Boyd. Enhancing sparsity by reweighted ℓ_1 minimization. *Journal of Fourier Analysis and Applications*, 14:877–905, 2008.
- [8] C.-C. Chang and C.-J. Lin. Libsvm: a library for support vector machines. *ACM Transactions on Intelligent Systems and Technology (TIST)*, 2(3):1–27, 2011.
- [9] X. Chen and C. T. Kelley. Convergence of the ediiis algorithm for nonlinear equations. *SIAM Journal on Scientific Computing*, 41(1):A365–A379, 2019.
- [10] D. Davis and D. Drusvyatskiy. Proximal methods avoid active strict saddles of weakly convex functions. *Foundations of Computational Mathematics*, 22(2):561–606, 2022.
- [11] D. Davis, D. Drusvyatskiy, and L. Jiang. Subgradient methods near active manifolds: saddle point avoidance, local convergence, and asymptotic normality. *arXiv preprint arXiv:2108.11832*, page 170, 2021.
- [12] D. Drusvyatskiy and A. S. Lewis. Optimality, identifiability, and sensitivity. *Mathematical Programming*, 147(1):467–498, 2014.
- [13] J. Eckstein and D. P. Bertsekas. On the douglas-rachford splitting method and the proximal point algorithm for maximal monotone operators. *Mathematical Programming*, 55:293–318, 1992.
- [14] M. Fazel, H. Hindi, and S. P. Boyd. Log-det heuristic for matrix rank minimization with applications to hankel and euclidean distance matrices. In *Proceedings of the 2003 American Control Conference, 2003.*, volume 3, pages 2156–2162. IEEE, 2003.

- [15] O. Fercoq and P. Richtárik. Accelerated, parallel, and proximal coordinate descent. *SIAM Journal on Optimization*, 25(4):1997–2023, 2015.
- [16] A. V. Fiacco. Sensitivity analysis for nonlinear programming using penalty methods. *Mathematical Programming*, 10(1):287–311, 1976.
- [17] A. Fu, J. Zhang, and S. Boyd. Anderson accelerated douglas–rachford splitting. *SIAM Journal on Scientific Computing*, 42(6):A3560–A3583, 2020.
- [18] P. Gong, C. Zhang, Z. Lu, J. Huang, and J. Ye. A general iterative shrinkage and thresholding algorithm for non-convex regularized optimization problems. In *International Conference on Machine Learning*, pages 37–45. PMLR, 2013.
- [19] W. L. Hare and A. S. Lewis. Identifying active manifolds. *Algorithmic Operations Research*, 2(2):75–82, 2007.
- [20] Q. Klopfenstein, Q. Bertrand, A. Gramfort, J. Salmon, and S. Vaïter. Local linear convergence of proximal coordinate descent algorithm. *Optimization Letters*, 18(1):135–154, 2024.
- [21] J. M. Lee. *Introduction to Smooth Manifolds*. Springer, 2013.
- [22] A. S. Lewis. Active sets, nonsmoothness, and sensitivity. *SIAM Journal on Optimization*, 13(3):702–725, 2002.
- [23] A. S. Lewis and S. J. Wright. A proximal method for composite minimization. *Mathematical Programming*, 158:501–546, 2016.
- [24] J. Liang, J. Fadili, and G. Peyré. Activity identification and local linear convergence of forward–backward-type methods. *SIAM Journal on Optimization*, 27(1):408–437, 2017.
- [25] M. S. Lobo, M. Fazel, and S. Boyd. Portfolio optimization with linear and fixed transaction costs. *Annals of Operations Research*, 152:341–365, 2007.
- [26] Z. Lu. Iterative reweighted minimization methods for ℓ_p regularized unconstrained non-linear programming. *Mathematical Programming*, 147(1-2):277–307, 2014.
- [27] V. Mai and M. Johansson. Anderson acceleration of proximal gradient methods. In *International Conference on Machine Learning*, pages 6620–6629. PMLR, 2020.
- [28] R. Mifflin and C. Sagastizábal. A vu-algorithm for convex minimization. *Mathematical Programming*, 104:583–608, 2005.
- [29] B. S. Mordukhovich. *Variational Analysis and Generalized Differentiation II: Applications*, volume 331. Springer, 2006.
- [30] W. Ouyang, Y. Peng, Y. Yao, J. Zhang, and B. Deng. Anderson acceleration for nonconvex admm based on douglas–rachford splitting. In *Computer Graphics Forum*, volume 39, pages 221–239. Wiley Online Library, 2020.
- [31] L. I. Rudin, S. Osher, and E. Fatemi. Nonlinear total variation based noise removal algorithms. *Physica D: Nonlinear Phenomena*, 60(1-4):259–268, 1992.

- [32] D. Scieur, A. d’Aspremont, and F. Bach. Regularized nonlinear acceleration. *Advances In Neural Information Processing Systems*, 29, 2016.
- [33] A. Shapiro. On a class of nonsmooth composite functions. *Mathematics of Operations Research*, 28(4):677–692, 2003.
- [34] A. Themelis and P. Patrinos. Douglas–rachford splitting and admm for nonconvex optimization: Tight convergence results. *SIAM Journal on Optimization*, 30(1):149–181, 2020.
- [35] R. Tibshirani. Regression shrinkage and selection via the lasso. *Journal of the Royal Statistical Society Series B: Statistical Methodology*, 58(1):267–288, 1996.
- [36] A. Toth and C. T. Kelley. Convergence analysis for anderson acceleration. *SIAM Journal on Numerical Analysis*, 53(2):805–819, 2015.
- [37] S. Vaiter, G. Peyré, and J. Fadili. Model consistency of partly smooth regularizers. *IEEE Transactions on Information Theory*, 64(3):1725–1737, 2017.
- [38] H. Wang, H. Zeng, J. Wang, and Q. Wu. Relating ℓ_p regularization and reweighted ℓ_1 regularization. *Optimization Letters*, 15(8):2639–2660, 2021.
- [39] S. J. Wright. Coordinate descent algorithms. *Mathematical Programming*, 151(1):3–34, 2015.